FEB 26 1993

ORNL
MASTER COPY

NUREG/CR–5922
ORNL/TM–12179

Modular High-Temperature Gas-Cooled Reactor Short-Term Thermal Response to Flow and Reactivity Transients

Prepared by
J. C. Cleveland

Oak Ridge National Laboratory

Prepared for
U.S. Nuclear Regulatory Commission

AVAILABILITY NOTICE

Availability of Reference Materials Cited in NRC Publications

Most documents cited in NRC publications will be available from one of the following sources:

1. The NRC Public Document Room, 2120 L Street, NW., Lower Level, Washington, DC 20555

2. The Superintendent of Documents, U.S. Government Printing Office, P.O. Box 37082, Washington, DC 20013-7082

3. The National Technical Information Service, Springfield, VA 22161

Although the listing that follows represents the majority of documents cited in NRC publications, it is not intended to be exhaustive.

Referenced documents available for inspection and copying for a fee from the NRC Public Document Room include NRC correspondence and internal NRC memoranda; NRC bulletins, circulars, information notices, inspection and investigation notices; licensee event reports; vendor reports and correspondence; Commission papers; and applicant and licensee documents and correspondence.

The following documents in the NUREG series are available for purchase from the GPO Sales Program: formal NRC staff and contractor reports, NRC-sponsored conference proceedings, international agreement reports, grant publications, and NRC booklets and brochures. Also available are regulatory guides, NRC regulations in the *Code of Federal Regulations*, and *Nuclear Regulatory Commission Issuances*.

Documents available from the National Technical Information Service include NUREG-series reports and technical reports prepared by other Federal agencies and reports prepared by the Atomic Energy Commission, forerunner agency to the Nuclear Regulatory Commission.

Documents available from public and special technical libraries include all open literature items, such as books, journal articles, and transactions. *Federal Register* notices, Federal and State legislation, and congressional reports can usually be obtained from these libraries.

Documents such as theses, dissertations, foreign reports and translations, and non-NRC conference proceedings are available for purchase from the organization sponsoring the publication cited.

Single copies of NRC draft reports are available free, to the extent of supply, upon written request to the Office of Administration, Distribution and Mail Services Section, U.S. Nuclear Regulatory Commission, Washington, DC 20555.

Copies of industry codes and standards used in a substantive manner in the NRC regulatory process are maintained at the NRC Library, 7920 Norfolk Avenue, Bethesda, Maryland, for use by the public. Codes and standards are usually copyrighted and may be purchased from the originating organization or, if they are American National Standards, from the American National Standards Institute, 1430 Broadway, New York, NY 10018.

DISCLAIMER NOTICE

This report was prepared as an account of work sponsored by an agency of the United States Government. Neither the United States Government nor any agency thereof, or any of their employees, makes any warranty, expressed or implied, or assumes any legal liability of responsibility for any third party's use, or the results of such use, of any information, apparatus, product or process disclosed in this report, or represents that its use by such third party would not infringe privately owned rights.

NUREG/CR-5922
ORNL/TM-12179
R1, R7, R8

Modular High-Temperature Gas-Cooled Reactor Short-Term Thermal Response to Flow and Reactivity Transients

Manuscript Completed: January 1993
Date Published: February 1993

Prepared by
J. C. Cleveland

Oak Ridge National Laboratory
Managed by Martin Marietta Energy Systems, Inc.

Oak Ridge National Laboratory
Oak Ridge, TN 37831-6285

Prepared for
Division of Systems Research
Office of Nuclear Regulatory Research
U.S. Nuclear Regulatory Commission
Washington, DC 20555
NRC FIN A9477
Under Contract No. DE-AC05-84OR21400

Abstract

The research reported here has been conducted at the Oak Ridge National Laboratory for the Nuclear Regulatory Commission's Division of Regulatory Applications of the Office of Nuclear Regulatory Research. The short-term thermal response of the Modular High-Temperature Gas-Cooled Reactor (MHTGR) is analyzed for a range of flow and reactivity transients. These transients include loss of forced circulation without scram, spurious withdrawal of a control rod group, moisture ingress, control rod and control rod group ejections, and a rapid core cooling event. For each event analyzed, an event description, a discussion of the analysis approach and assumptions, and results are presented. When possible, results of these analyses are compared with those presented by the designers in the MHTGR Preliminary Safety Information Document and in the MHTGR Probabilistic Risk Assessment. The importance of inherent safety features is illustrated, and conclusions are presented regarding the safety performance of the MHTGR. Recommendations are made for a more in-depth examination of MHTGR response for some of the analyzed transients. The coupled heat transfer-neutron kinetics model is described in detail in Appendix A.

Contents

	Page
Abstract	iii
List of Figures	vii
List of Tables	ix
1 Introduction and Purpose	1
2 Summary Description of the MHTGR	2
3 Summary of Plant Control and Protection System Actions for Flow and Reactivity Transients	4
4 Examination of Response to a LOFC Without Scram	5
4.1 Event Description	5
4.2 Discussion of Relevant Experience in a Gas-Cooled Reactor	5
4.3 Analysis Approach and Assumptions	5
4.4 Results of LOFC	5
5 Examination of Response to Moisture Ingress	8
5.1 Event Description	8
5.2 Analysis Approach and Assumptions	8
5.3 Results of Moisture Ingress Analyses	8
6 Examination of Response to Control Rod Group Withdrawal Without Scram (With Constant Core Flow)	12
6.1 Event Description	12
6.2 Analysis Approach and Assumptions	12
6.3 Results of Response to Control Rod Group Withdrawal Without Scram (Constant Core Flow) Analyses	12
7 Examination of Response to Control Rod Group Withdrawal Without Scram (With Decreasing Core Flow)	14
7.1 Event Description	14
7.2 Analysis Approach and Assumptions	14
7.3 Results of Response to Control Rod Group Withdrawal Without Scram (Decreasing Core Flow) Analyses	14
8 Examination of Response to Control Rod Group Withdrawal With Scram	16
8.1 Event Description	16
8.2 Analysis Approach and Assumptions	16
8.3 Results of Control Rod Group Withdrawal Transient With Scram Analyses	16
9 Examination of Reactor Response to a Rapid Core Cooling Without Scram	19
9.1 Event Description	19
9.2 Analysis Approach and Assumptions	19

9.3 Results of Rapid Core Cooling Without Scram Analyses 19

10 Examination of Response to a Control Rod Ejection Transient 24

10.1 Event Description 24
10.2 Analysis Approach and Assumptions 24
10.3 Results of Control Rod Ejection Analyses 24

11 Examination of Response to a Control Rod Group Ejection Transient 27

11.1 Event Description 27
11.2 Analysis Approach and Assumptions 27
11.3 Results of Control Rod Group Ejection Analyses 27

12 Conclusions and Recommendations 29

References 31

Appendix A Description of the Coupled Neutron Kinetics-Core Heat Transfer Dynamics Model 32

References 38

Appendix B Approximate Analytical Methods for Predicting Power and Fuel Temperature Response for Large Step Reactivity Insertions 39

References 42

List of Figures

Figure		Page
2.1	MHTGR nuclear steam supply system	3
4.1	*(a)* Power, flux, and temperature response during LOFC without scram; *(b)* reactivity response during LOFC without scram	6
5.1	*(a)* Temperature and power response during moisture group withdrawal without scram (constant core flow); *(b)* reactivity response during moisture ingress	10
5.2	*(a)* Temperature and power response during moisture ingress event with shutdown of helium circulator at 120 s; *(b)* reactivity response during moisture ingress event with shutdown of helium circulator at 120 s	11
6.1	*(a)* Temperature and power response during control rod group withdrawal without scram (constant core flow); *(b)* reactivity response during control rod group withdrawal without scram (constant core flow)	13
7.1	*(a)* Temperature and power response during control rod group withdrawal without scram (decreasing core flow); *(b)* reactivity response during control rod group withdrawal without scram (decreasing core flow)	15
8.1	*(a)* Temperature and power response during control rod group withdrawal with scram (constant core flow); *(b)* reactivity response during control rod group withdrawal with scram (constant core flow)	17
8.2	*(a)* Temperature and power response during control rod group withdrawal with scram (decreasing core flow); *(b)* reactivity response during control rod group withdrawal with scram (decreasing core flow)	18
9.1	*(a)* Temperature and power response during rapid core cooling event; *(b)* reactivity response during rapid core cooling event	20
9.2	*(a)* Temperature and power response during rapid core cooling event (fuel and moderator temperature coefficient arbitrarily reduced by $2 \times 10^{-5}/°C$); *(b)* reactivity response during rapid core cooling event (fuel and moderator temperature coefficients arbitrarily reduced by $2 \times 10^{-5}/°C$)	21
9.3	Stable period vs reactivity	22
9.4	*(a)* Temperature and power response during rapid core cooling event (initial power = 100 kW); *(b)* reactivity response during rapid core cooling event (initial power = 100 kW)	23
10.1	*(a)* Temperature and power response during control rod ejection event (10-s rod ejection time); *(b)* reactivity response during control rod ejection event (10-s rod ejection time)	25
10.2	*(a)* Temperature and power response during control rod ejection event (1.0-s rod ejection time); *(b)* reactivity response during control rod ejection event (1.0-s rod ejection time)	26

11.1 *(a)* Temperature and power response during control rod group ejection event; *(b)* reactivity response during control rod group ejection event 28

A.1 *(a)* Basic triangular cell of MHTGR fuel block; *(b)* equivalent cylindrical cell 34

List of Tables

Table		Page
2.1	Summary design parameters of the reference MHTGR	2
3.1	Safety protection subsystem trip levels and set points	4
5.1	Moisture ingress reactivity vs time for steam generator tube break	9
A.1	Delayed neutron precursor data	33

1 Introduction and Purpose

The Modular High-Temperature Gas-Cooled Reactor (MHTGR) is an advanced reactor concept being developed under a cooperative program involving the U.S. Department of Energy, the nuclear industry, and utilities. The conceptual design is being reviewed by the Nuclear Regulatory Commission (NRC). As part of a research program to support the NRC's review activities, Oak Ridge National Laboratory (ORNL) has analyzed the short-term thermal response of the reactor for a range of flow and reactivity transients. Certain actions of the plant control and protection system have been assumed not to function to examine the response to extremely unlikely events.

This work has been performed to (1) enable comparisons with results obtained by the design team and (2) search for conditions that lead to more severe transients than previously identified. The following events, which cover a wide range of flow and reactivity transients, were selected for examination:

1. loss of forced circulation (LOFC) without scram,
2. moisture ingress,
3. control rod group withdrawal without scram (with constant core coolant flow),
4. control rod group withdrawal without scram (with decreasing core coolant flow),
5. control rod group withdrawal with scram,
6. rapid core cooling without scram,
7. control rod ejection, and
8. control rod group ejection.

This selection was based on a review of transients [both design-basis and beyond-design-basis accidents including Safety-Related Design Conditions (SRDCs)] presented in the preliminary safety and information document (PSID), although the selection was not limited to events discussed in the PSID. Specifically, events 3, 4, 6, 7, and 8 in the previous list were not analyzed in the PSID.

To the extent possible at this stage of investigations, the results presented are independent of the designer's effort. However, values for important neutronic parameters—cross sections, axial flux profile, temperature coefficients of reactivity, reactivity worth of moisture, control rod worth, delayed neutron parameters, and neutron generation time—used in these analyses were obtained from the designer, thereby limiting the degree of independence of this work. Investigations of the accuracy of these parameters and their uncertainty are under way, and when these activities are complete, additional analyses will be conducted. Understanding the effects of uncertainties in these parameters is essential.

For this examination, fuel temperatures below 1600°C are considered acceptable.[1] Investigations of the validity of this temperature range, as well as reviews of plans by the developer to further substantiate acceptable fission product retention in fuel at temperatures in this range, are also under way.

Unless otherwise noted, end-of-equilibrium cycle fuel and moderator temperature coefficients of reactivity were used because they are the least negative values reported.

2 Summary Description of the MHTGR

The reference MHTGR plant design consists of four reactor modules each rated at 350 MW(t) (see Fig. 2.1) coupled to two steam turbine generators yielding a net power output of about 550 MW(e). The reactor design utilizes the basic HTGR features of ceramic fuel, helium coolant, and a graphite moderator. The coated fuel particles are compacted in a graphite matrix into fuel rods and are loaded in hexagonal graphite blocks. Reactor heat is transferred by a once-through steam generator to produce high-temperature, high-pressure steam. Table 2.1 summarizes major design parameters.

The reactor vessel is similar in size, weight, and material of construction to existing large light-water reactor vessels. The reactor vessel contains the reactor core and reflector, neutron control material, core support structures, and a shutdown cooling heat exchanger with its motor-driven helium circulator. The steam generator vessel houses the helically coiled steam generator bundle as well as the motor-driven main circulator. The reactor vessel is uninsulated to provide for decay heat removal under LOFC conditions to the passive reactor cavity cooling system (RCCS), which circulates outside air by natural circulation within enclosed panels surrounding the reactor vessel.

Table 2.1 Summary design parameters of the reference MHTGR

Thermal power	350 MW(t)
Steam conditions	538°C (1000°F) 163 atm (24,500 psig)
Core exit helium temperature	687°C (1268°F)
Core inlet helium temperature	258°C (497°F)
Core power density	5.9 W/cm^3
Equilibrium fuel burnup	82,460 MWd/T

ORNL-DWG 89-4877A ETD

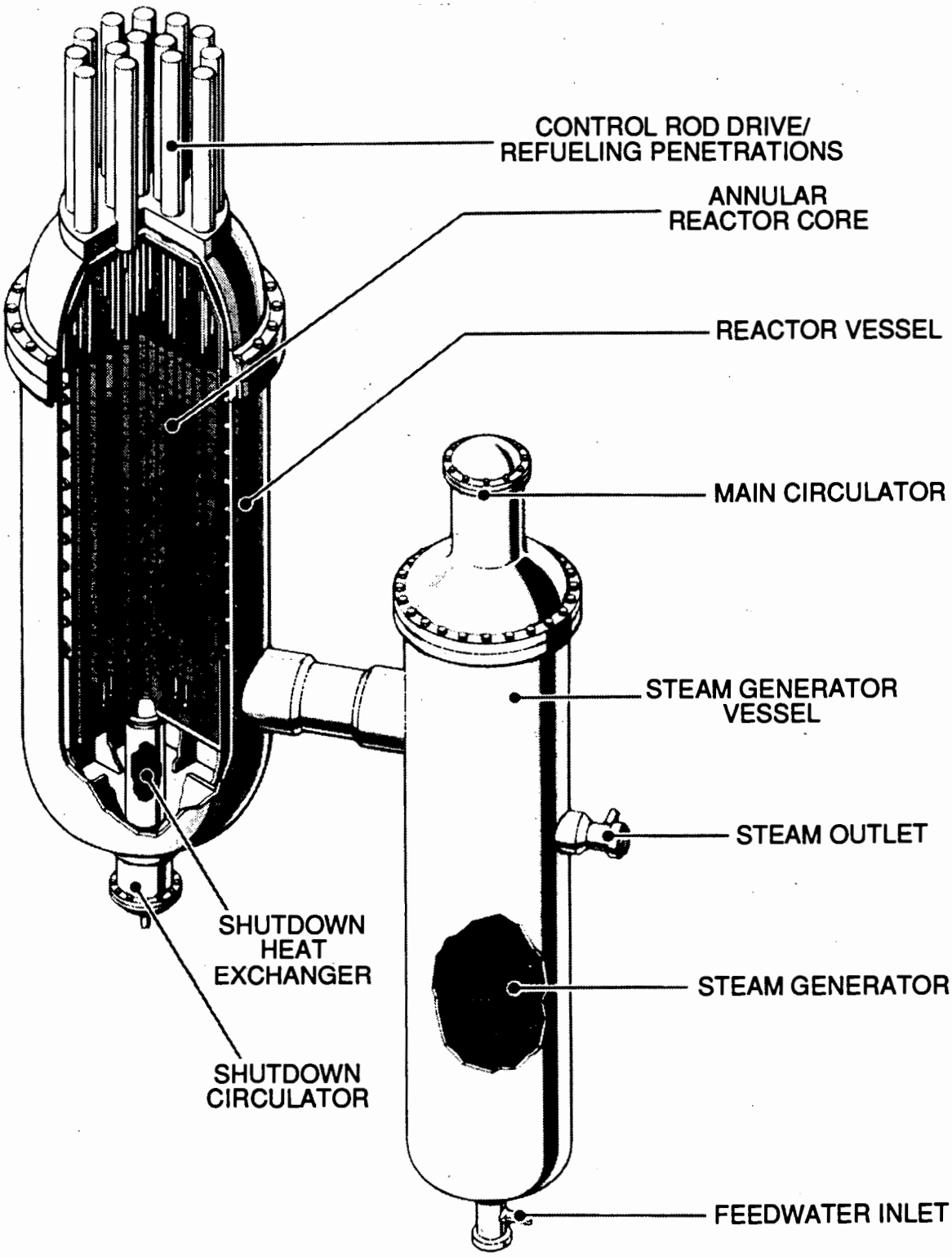

Figure 2.1 MHTGR nuclear steam supply system

3 Summary of Plant Control and Protection System Actions for Flow and Reactivity Transients

Several actions are designed into the plant control and protection systems to limit or terminate off-normal events involving flow and reactivity changes. These include the following:

1. the neutron flux controller;
2. a control rod trip on each of the following signals:
   - high neutron flux to helium mass flow ratio (1.40),
   - high primary system pressure (7.00 MPa),
   - low primary system pressure (5.76 MPa),
   - high steam generator inlet helium temperature (746°C), and
   - high primary coolant moisture concentration (1000 ppmv);
3. insertion of reserve shutdown material on each of the following signals:
   - high neutron flux to circulator speed ratio (1.80 with 30-s time delay), and
   - high primary system pressure (7.00 MPa);
4. a manual control rod or reserve shutdown system trip by the operator; and
5. main loop shutdown (shutoff of the helium circulator and secondary side of the steam generator) on each of the following signals:
   - high primary system pressure (7.00 MPa),
   - high or low circulator speed, and
   - low primary system pressure (5.76 MPa).

The safety protection subsystem set points are summarized in Table 3.1, based on information presented in the PSID. Upon initiation of the reactor trip signal, all control rods in the outer reflector are inserted. The reserve shutdown material is released into the core (with an appropriate time delay) if the outer control rods fail to trip when commanded or when excessive water enters the core.

In the events analyzed in the following sections, some or all of these functions are assumed not to occur.

Table 3.1 Safety protection subsystem trip levels and set points

	Protection system setting
Reactor trip using outer control rods	
Neutron flux (%) to helium mass flow (%) ratio	1.40
Primary coolant pressure—high	7.00 MPa (1015 psia)
Primary coolant pressure—low and neutron flux >10%	5.76 MPa (835 psia)
Steam generator helium inlet temperature	746°C (1375°F)
Primary coolant moisture concentration	1000 ppmv
Reactor trip using reserve shutdown system	
Neutron flux (%) to circulator speed (%) ratio	1.8 with a 30-s time delay
Primary coolant pressure	7.00 MPa (1015 psia)

4 Examination of Response to a LOFC Without Scram

4.1 Event Description

For this event, it is assumed that power to the circulator motor drive is lost with the reactor initially operating at full power and flow conditions. Further, it is assumed that there is no reactor scram (normally if this event occurred, the safety protection subsystem would scram the reactor on a high power-to-flow ratio signal) and that the shutdown cooling system does not operate. For the time interval analyzed here, this event is similar to SRDC-1 and -2 presented in the PSID except that no insertion of control rods or reserve shutdown material is considered here.

4.2 Discussion of Relevant Experience in a Gas-Cooled Reactor

The staff of the Arbeitsgemeinschaft Versuchsreaktor (AVR) pebble bed HTGR in Jülich, Federal Republic of Germany, have conducted a series of tests demonstrating the safe response of that reactor to a LOFC without scram event.[2] Although the AVR is a relatively low-power-level reactor [46 MW(t), 15 MW(e)], it possesses many features also incorporated into modular gas-cooled reactors [low power density, low enriched uranium (LEU) fuel, coated fuel particles, negative temperature coefficient of reactivity, and the capability for passive removal of afterheat through the reactor vessel wall]. The AVR, therefore, permits experimental investigations and demonstrations of important features pertinent to modular gas-cooled reactor performance and safety.

In one LOFC test[3] with the reactor initially at 96% power, both helium circulators were intentionally stopped, and the main gas valves at the circulator outlets were closed. No scram signal (which, at the AVR is based on high neutron flux, high rate of change of flux, or high or low helium pressure) was generated because none of the scram set points was exceeded. When the helium circulators were stopped, the reactor quickly went subcritical because of the increasing fuel temperature and the strongly negative temperature coefficient of reactivity. The shutdown rods were not inserted to demonstrate that this function is not needed. The natural convection of helium allowed some of the afterheat to be removed by the steam generators. Heat was also removed by the interspace cooler (which cools a biological shield between the inner and outer reactor vessels) and by radiation from the wall of the outer vessel. After ~23.5 h, because of decreasing temperatures and decreasing ^{135}Xe concentration, the reactor again went critical, with the power peaking at ~1.8 MW (~4% of full power) and stabilizing at <1% of full power. The experiment was terminated by inserting the control rods. Until this time, there had been no operator intervention. Temperatures in the pebble bed itself were not measured. However, from other temperature measurements in the reflector regions, it was inferred that the maximum fuel temperature increased only ~65°C during this transient,[4] thereby limiting the maximum fuel temperature to ~1200 to 1250°C, well below the temperature for the onset of fission product release.

4.3 Analysis Approach and Assumptions

For analysis of the MHTGR response to this event, the circulator is assumed to coast down in 90 s after the loss of electrical power. Core flow is calculated assuming the volumetric flow is proportional to circulator speed. The shutdown cooling system was assumed not to operate. This event was analyzed using the coupled neutron kinetics-heat transfer code described in Appendix A. For the relatively short time interval considered, heat losses from the core through the reactor vessel by conduction, convection, and radiation to the reactor cavity were neglected. Values for fuel and moderator temperature coefficients of reactivity were obtained from the PSID and from Ref. 5, as discussed in Appendix A. Temperature coefficients of reactivity for end-of-equilibrium cycle conditions were used because they are least negative. Also, end-of-cycle values for delayed neutron fractions, weighted according to ^{235}U, ^{233}U, and ^{239}Pu fission rates, were used (see Appendix A).

4.4 Results of LOFC Without Scram Analyses

Figure 4.1(*a*) shows the computed time response of the neutron flux, the total core power (including decay power), the average core temperature, and the maximum temperature in the average fuel column, as well as the assumed core coolant flow rate. With loss of power to the circulator (at t = 60 s), the flow reduction caused by circulator coastdown results in increases in fuel and moderator temperatures because the thermal power exceeds the rate of heat removal by convection. The corresponding reactivity components caused by changes in xenon concentration and in fuel and moderator temperatures are shown in Fig. 4.1(*b*). The reactivity component due to the moderator temperature increase is positive because of the slightly positive moderator temperature coefficient at normal operating temperatures. However, the reactivity component caused by the fuel heatup is sufficiently negative to drive the reactor subcritical. The reactor reaches decay power levels

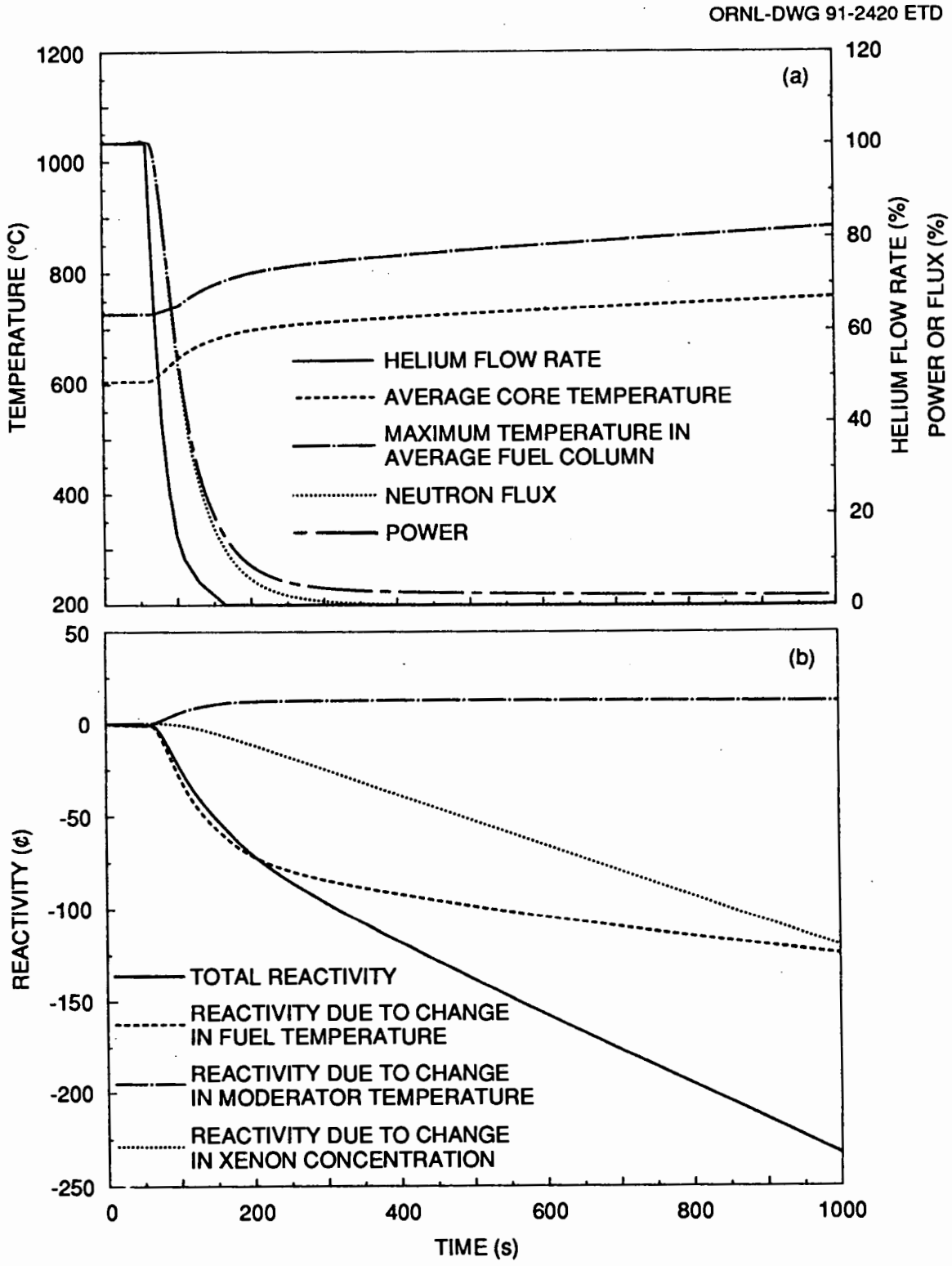

Figure 4.1 ***(a)*** **Power, flux, and temperature response during LOFC without scram;** ***(b)*** **reactivity response during LOFC without scram**

~300 s after initiation of the event. This result is consistent with the discussion of results presented in Ref. 6. Because of the corresponding decrease in neutron flux [see Fig. 4.1(*a*)], the ^{135}Xe concentration increases because of the reduced xenon burnout rate causing an additional negative reactivity component as shown in Fig. 4.1(*b*).

As time continues beyond the interval analyzed here, the higher than normal core temperatures and the increasing xenon poisoning following the subcriticality are sufficient to hold the reactor subcritical for many hours. This allows a long time to insert the control rods or reserve shutdown material. If either of these actions is taken before recriticality, maximum fuel temperatures would be below those for a loss-of-coolant accident (LOCA) (also called a depressurized conduction cooldown accident) because the natural convection of helium in the LOFC would tend to cool the core somewhat faster than for the LOCA. (For a LOFC event, the reactor is assumed to remain pressurized.)

After several hours, the xenon poisoning will decrease as the ^{135}Xe decays; the core will cool by heat dissipation through the reactor vessel wall; and, if either the control rods or the reserve shutdown material still are not inserted, a recriticality will occur. (Analysis of this longer term response requires coupling of the neutron kinetics model with a heat transport model, which includes heat dissipation through the reactor vessel wall.) The recriticality would increase the temperatures sufficiently to again drive the reactor subcritical.

As the ^{135}Xe decays, if either the control rods or the reserve shutdown material is still not inserted, the temperature will rise enough to provide negative reactivity equal to that lost through decay of xenon. Because the xenon will ultimately decay to zero, the temperature will rise to some value higher than its usual full-power level (~600°C). Based on the end-of-equilibrium cycle core isothermal temperature coefficients (with reflector heatup) reported in the PSID, to counter this reactivity normally held by xenon during reactor operation requires an increase in the average core temperature of ~800°C. The reactor would ultimately stabilize in a critical condition generating just enough power to maintain core temperatures at that level, which results in zero net reactivity. The power generated will precisely equal the power dissipated by losses through the vessel wall; in fact, the power generation will be determined by the ability of the RCCS to dissipate heat at reactor temperatures, which provide zero net reactivity.

5 Examination of Response to Moisture Ingress

5.1 Event Description

The short-term response of the reactor to the reactivity introduced into the core by the rupture of a single steam generator tube is analyzed. In response to an increase in neutron flux caused by moisture entering the core, the neutron flux controller attempts to maintain constant power by driving control rods into the core. Also, the safety protection subsystem is designed to trip the reactor on a high power-to-flow ratio or on a high primary coolant-pressure signal. As an investment protection function, the reactor is also tripped when a high moisture level is sensed. None of these functions have been assumed to be implemented for the analyses reported here.

This event is similar to SRDC-6 presented in the PSID except that the trip of the control rods is not considered here. For SRDC-6, both the mitigating actions of the neutron flux controller and the moisture monitor trip signal are ignored because they are not safety related; the reactor is, however, scrammed on a high power-to-flow signal, which is safety related.

5.2 Analysis Approach and Assumptions

According to 11.1–9 of the PSID the primary system circulating helium inventory is 1621 kg. Therefore, with a helium flow rate of 157.4 kg/s at full-power conditions, the helium transport time through the primary system is 10.3 s. Thus, for this analysis, it was assumed that the moisture from the ruptured steam generator tube reaches the core in 5 s. Further, the volume of core voids (coolant channels) is ~10.7 m^3, resulting in a transport time of ~0.3 s through the core. According to the PSID, moisture is introduced into the primary system initially at a rate of 27.2 kg/s, reducing to a quasi-steady leak rate of 5.7 kg/s in 1.5 s. For conservatism in these analyses, the moisture was assumed to enter the primary system at 27.2 kg/s for the entire initial 1.5 s and at 5.7 kg/s thereafter. It was assumed that the steam passes through the core as a front and that no moisture (or H_2) collects in the core. The primary system mass flow rate was assumed to remain constant.

The reactivity worth of water was obtained from Ref. 5 to be ~0.0075% $\Delta\rho$/kg (valid to ~400 kg). Beginning-of-cycle values for water reactivity worth were used because these are somewhat greater than end-of-cycle values. Based on the above, the values shown in Table 5.1 were obtained for the time dependence of the amount of water in the core and the associated reactivity worth. After six passes of the front of higher moisture concentration through the core, which results from the higher ingress rate during the initial 1.5 s, homogeneous mixing of moisture and helium in the primary system was assumed. Core cooling, caused by the endothermic reaction of water with graphite, was neglected.

The end-of-cycle neutron kinetics parameters and temperature coefficients provided by the designer were used. The influence of moisture on the temperature coefficient was not included in these values provided by the designer. The transient was analyzed using the model described in Appendix A.

5.3 Results of Moisture Ingress Analyses

Figure 5.1(*a*) shows the response of core power and temperatures to the moisture ingress. Figure 5.1(*b*) shows the response of the core reactivity and its various components. The spikes in the power response result from repeated passes through the core of the front of higher concentration of moisture, which resulted from the higher ingress rate during the initial 1.5 s of the ingress. The initial power increase to 116% is a result of the ramp insertion of 0.0612% reactivity (12.8¢) over 0.3 s. The prompt jump approximation, $\Phi/\Phi_o = \beta(1 - \rho)/(\beta - \rho)$, for a step insertion of this amount of reactivity would yield a power increase to 114.5%. The other spikes caused by repeated passes of the front of higher moisture concentration through the core are similar in magnitude. Beyond 60 s, the assumption of homogeneous mixing of the steam in the primary system results in a smoother power response. The set point for reactor trip on high primary coolant moisture concentration (1000 ppmv) would be reached a few seconds into the transient. Only 12 kg of moisture need be uniformly distributed through the circulating helium to reach this scram set point. However, a scram was not considered in the analyses shown in Fig. 5.1(*a*) and (*b*). The high power-to-flow trip level of 1.4 is reached about 210 s after initiation of the leak.

The results presented in the PSID for this transient (Design-Basis Event No. 6) are considerably different than those shown in Fig. 5.1(*a*). The PSID predicts a peak power of ~180% occurring only 9 s after accident initiation, with a scram on high moisture content at ~22 s after the onset of the leak. The reason for the much more rapid power increase reported in the PSID was determined to be General Atomics' conservative assumption that moisture

Table 5.1 Moisture ingress reactivity vs time for steam generator tube break

Time after break (s)	Moisture in core (kg)	Reactivity worth (% Δρ)
0.0	0.0	0.0
5.0	0.0	0.0
5.1	2.72	0.0204
5.2	5.44	0.0408
5.3	8.16	0.0612
6.5	8.16	0.0612
6.6	6.01	0.0451
6.7	3.86	0.0290
6.8	1.71	0.0128
15.3	1.71	0.0128
15.4	1.71 + 2.72 = 4.43	0.0332
15.5	1.71 + 5.44 = 7.15	0.0536
15.6	1.71 + 8.16 = 9.87	0.0740
16.8	1.71 + 8.16 = 9.87	0.0740
16.9	1.71 + 6.01 = 7.72	0.0579
17.0	1.71 + 3.86 = 5.57	0.0418
17.1	1.71 + 1.71 = 3.42	0.0257
25.6	2 × 1.71 = 3.42	0.0257
25.7	2 × 1.71 + 2.72 = 6.14	0.0461
25.8	2 × 1.71 + 5.44 = 8.86	0.0665
25.9	2 × 1.71 + 8.16 = 11.58	0.0869
27.1	2 × 1.71 + 8.16 = 11.58	0.0869
27.2	2 × 1.71 + 6.01 = 9.43	0.0707
27.3	2 × 1.71 + 3.86 = 7.28	0.0546
27.4	3 × 1.71 = 5.13	0.0385
35.9	3 × 1.71 = 5.13	0.0385
36.0	3 × 1.71 + 2.72 = 7.85	0.0589
36.1	3 × 1.71 + 5.44 = 10.57	0.0793
36.2	3 × 1.71 + 8.16 = 13.29	0.0997
37.4	3 × 1.71 + 8.16 = 13.29	0.0997
37.5	3 × 1.71 + 6.01 = 11.14	0.0836
37.6	3 × 1.71 + 3.86 = 8.99	0.0674
37.7	4 × 1.71 = 6.84	0.0513
46.2	4 × 1.71 = 6.84	0.0513
46.3	4 × 1.71 + 2.72 = 9.56	0.0717
46.4	4 × 1.71 + 5.44 = 12.28	0.0921
46.5	4 × 1.71 + 8.16 = 15.00	0.1125
47.7	4 × 1.71 + 8.16 = 15.00	0.1125
47.8	4 × 1.71 + 6.01 = 12.85	0.0964
47.9	4 × 1.71 + 3.86 = 10.70	0.0803
48.0	5 × 1.71 = 8.55	0.0641
56.5	5 × 1.71 = 8.55	0.0641
56.6	5 × 1.71 + 2.72 = 11.27	0.0845
56.7	5 × 1.71 + 5.44 = 13.99	0.1049
56.8	5 × 1.71 + 8.16 = 16.71	0.1253
58.0	5 × 1.71 + 8.16 = 16.71	0.1253
58.1	5 × 1.71 + 6.01 = 14.56	0.1092
58.2	5 × 1.71 + 3.86 = 12.41	0.0931
58.3	6 × 1.71 + 10.26	0.0770
65.0	10.85	0.0814
95.0	15.81	0.1186
125.0	20.77	0.1558
185.0	30.69	0.2302
245.0	40.61	0.3046

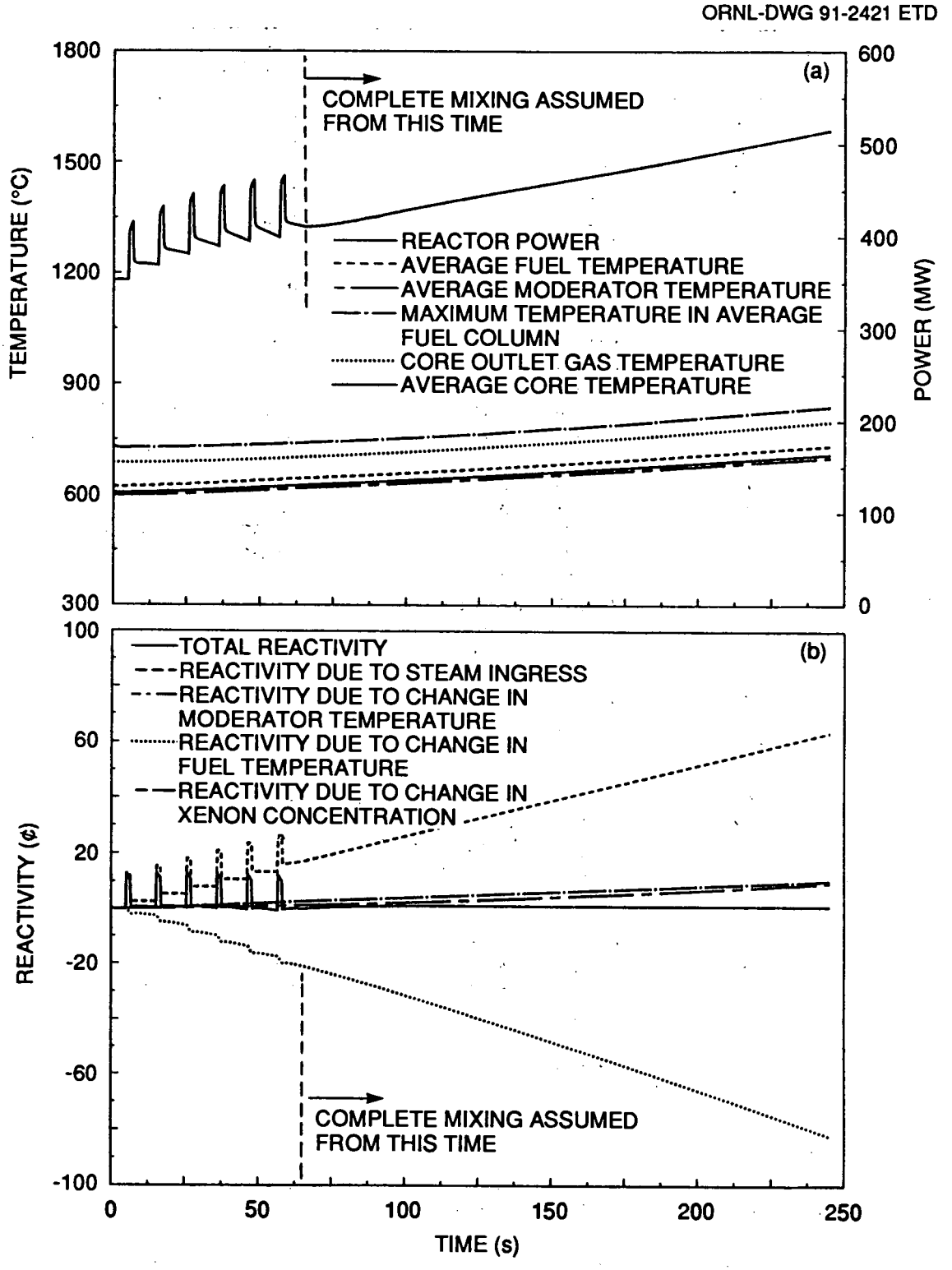

Figure 5.1 ***(a)*** **Temperature and power response during moisture group withdrawal without scram (constant core flow);** ***(b)*** **reactivity response during moisture ingress**

that enters the core mainly collects there rather than passing through.

The reactor power increase for this moisture ingress event can be terminated simply by stopping the helium circulator. Figure 5.2 shows that the response assuming circulator shutdown is initiated 120 s after rupture of the steam generator tube. For a moisture ingress event, the safety protection subsystem would initiate a circulator trip as part of a main loop shutdown resulting from a high primary system pressure signal. Determination of the timing of such a trip signal for this event requires more detailed modeling of the system.

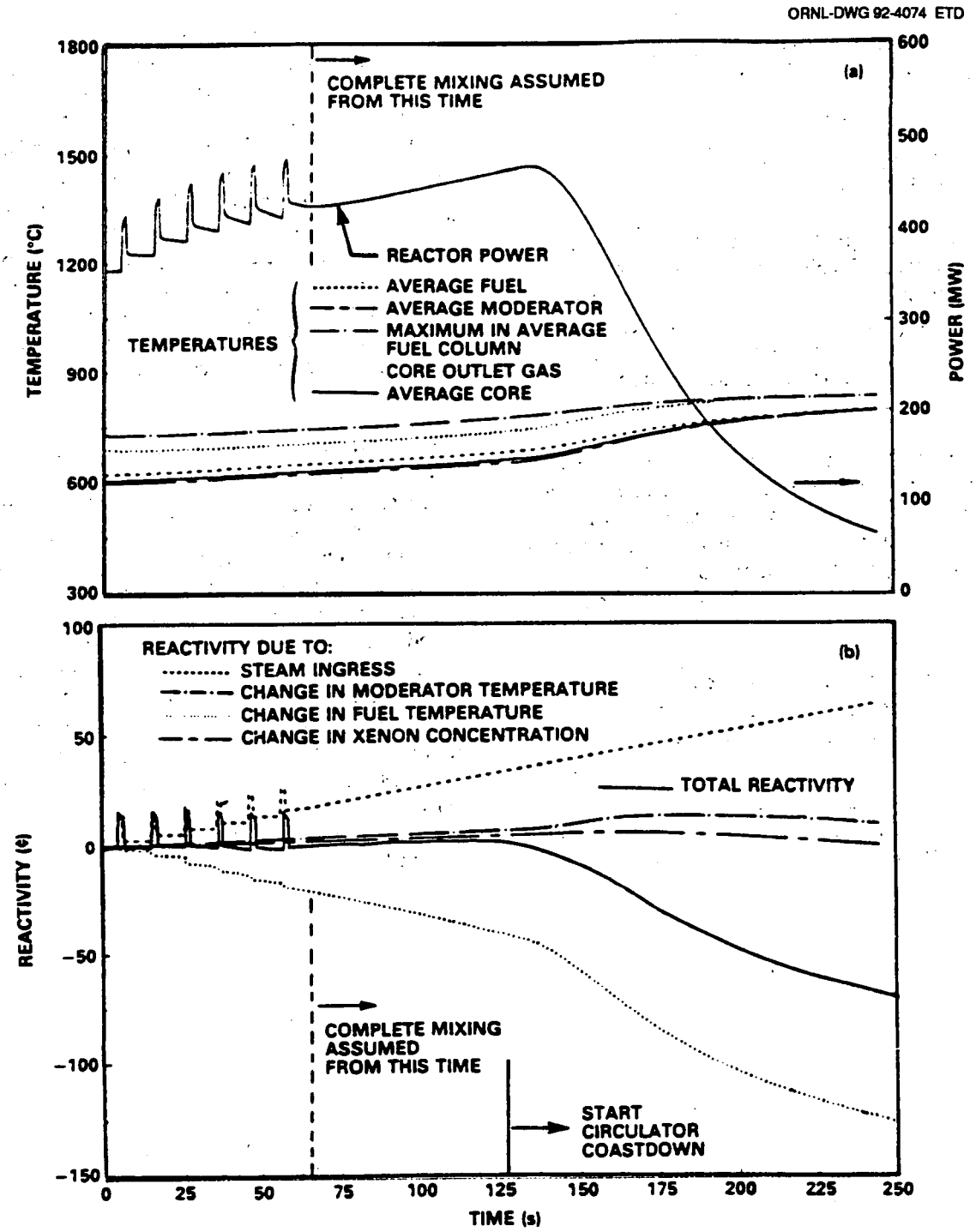

Figure 5.2 *(a)* **Temperature and power response during moisture ingress event with shutdown of helium circulator at 120 s;** *(b)* **reactivity response during moisture ingress event with shutdown of helium circulator at 120 s**

6 Examination of Response to Control Rod Group Withdrawal Without Scram (with Constant Core Flow)

6.1 Event Description

This event involves the accidental withdrawal of the control rod group of highest worth without action of the neutron flux controller. The reactor would scram on a high power-to-flow signal or on another scram signal (see Table 3.1); however, no scram was treated in this analysis.

6.2 Analysis Approach and Assumptions

The worth of the most reactive rod group was taken as 2.5% $\Delta\rho$, as stated in the PSID. The rod group was assumed to be fully initially inserted and to be withdrawn in 260 s. This time for full withdrawal was obtained from the PSID. The relation for rod worth vs distance inserted, provided by General Atomics, was used in this analysis.*

Normally, the main steam temperature controller would reduce circulator speed in an attempt to maintain the main steam temperature at its set point; for this analysis, however, this action was ignored (but see Sect. 7), and the circulator speed was assumed to remain constant. Also, the core inlet temperature was assumed to remain constant.

End-of-equilibrium cycle temperature coefficients and neutron kinetics parameters from the PSID were used, and the event was analyzed with the model described in Appendix A.

*J. C. Cleveland, Oak Ridge National Laboratory, personal communication with A. Baxter, General Atomics, June 1987.

6.3 Results of Response to Control Rod Group Withdrawal Without Scram (Constant Core Flow) Analyses

Figure 6.1(*a*) shows the response of core power and temperatures for this control rod group withdrawal transient (accident initiation was assumed to occur at 60 s). Figure 6.1(*b*) shows the response of the core reactivity and its various components. The high neutron flux-to-helium mass flow ratio of 1.5 would be reached ~78 s after accident initiation [at 138 s on Fig. 6.1(*a*)]; at this time, the average fuel temperature has increased to only 670°C, a 50°C increase above normal operating temperature. However, if the control rods or the reserve shutdown material are not inserted until several minutes into the transient, centerline temperatures in the average fuel column will exceed the 1600°C limit for onset of fission product release.

For the 30-min time interval analyzed, the xenon makes a positive reactivity contribution because of the burnout of ^{135}Xe at the higher flux. The power will approach a final value for which the increases in fuel and moderator temperatures result in a negative reactivity feedback just sufficient to balance the positive reactivity of 2.5% $\Delta\rho$ inserted by control rod withdrawal and the reactivity associated with the change in xenon concentration. The power level will be higher for this case, which involves constant core flow, than in the case for which core flow is assumed to be reduced to zero by the plant control system. The reactor will generate just the power required to hold core temperatures high enough to yield zero net reactivity under whatever flow conditions exist, and less power is required to hold temperatures at this elevated level if no heat is removed by forced convection.

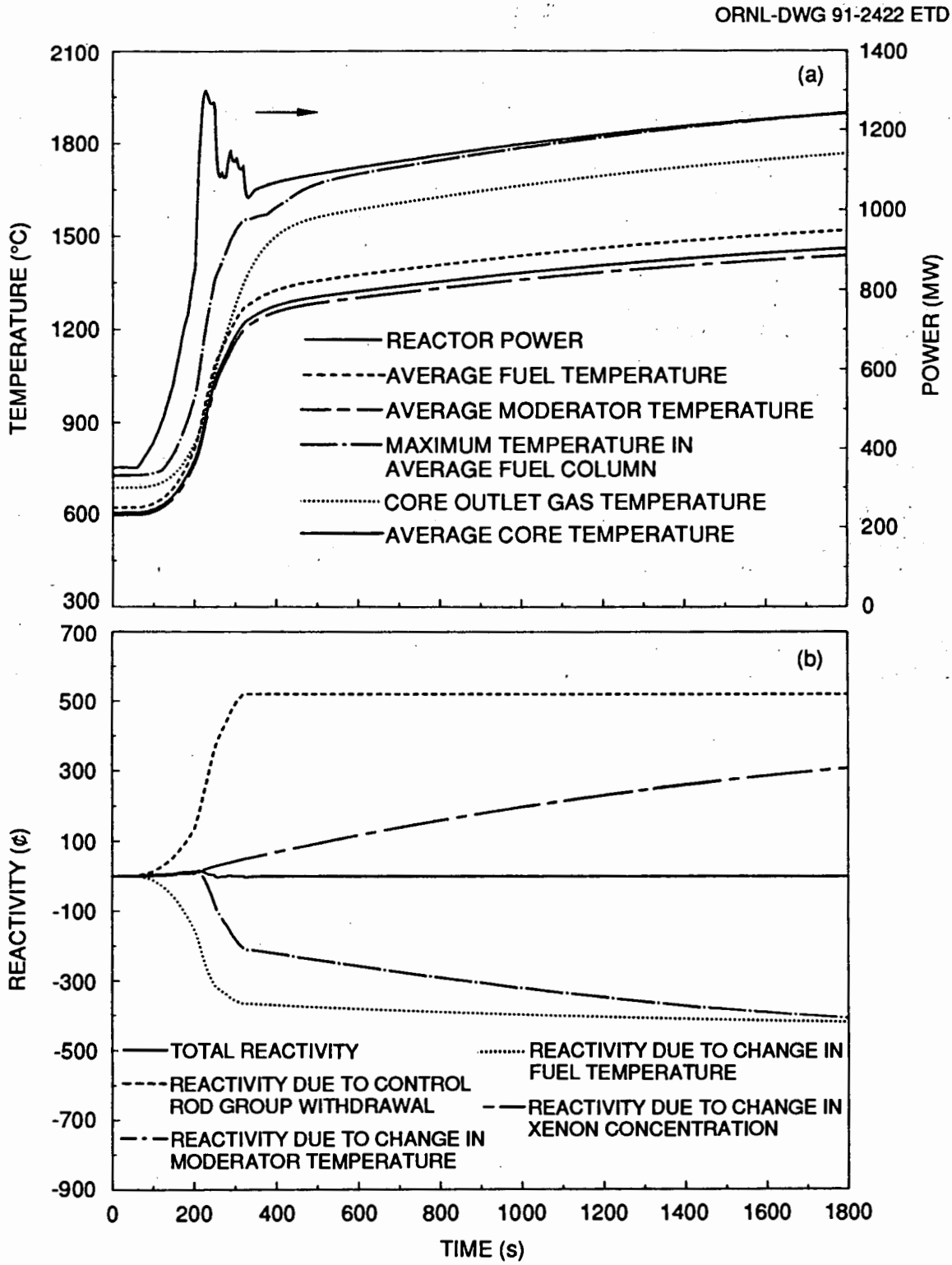

Figure 6.1 *(a)* **Temperature and power response during control rod group withdrawal without scram(constant core flow);** *(b)* **reactivity response during control rod group withdrawal without scram (constant core flow)**

7 Examination of Response to Control Rod Group Withdrawal Without Scram (with Decreasing Core Flow)

7.1 Event Description

The event analyzed here is similar to that discussed in Sect. 6 because it involves accident withdrawal of the control rod group of highest worth without action of the neutron flux controller. Again, the reactor is assumed not to scram. This case differs from that described in Sect. 6 because the effect of the main steam temperature controller is approximated by considering a decreasing circulator speed and core flow rate.

7.2 Analysis Approach and Assumptions

The assumptions for this case are the same as the case described in Sect. 6 except the core flow is assumed to decrease because of the action of the main steam temperature controller attempting to maintain main steam temperature at its set point. For these initial analyses, the rate at which the main steam temperature controller was assumed to decrease circulator speed was estimated from system analyses presented in Ref. 7 for a similar control system employed at the Fort St. Vrain reactor. The flow was assumed to decrease by 25% of full flow per 100 s, reaching zero flow by 400 s. The shutdown cooling system was assumed not to operate. The event was analyzed with the model described in Appendix A.

7.3 Results of Response to Control Rod Group Withdrawal Without Scram (Decreasing Core Flow) Analyses

Figure 7.1(*a*) shows the response of core power and temperatures for this control rod group withdrawal transient. Figure 7.1(*b*) shows the response of the core reactivity and its components. The effect of the decreasing core flow itself tends to increase core temperatures contributing a negative reactivity feedback. The result is a smaller power excursion than that experienced in the case for which core flow was held constant. The reactor is driven subcritical ~185 s after event initiation [245 s on Fig. 7.1(*a*)].

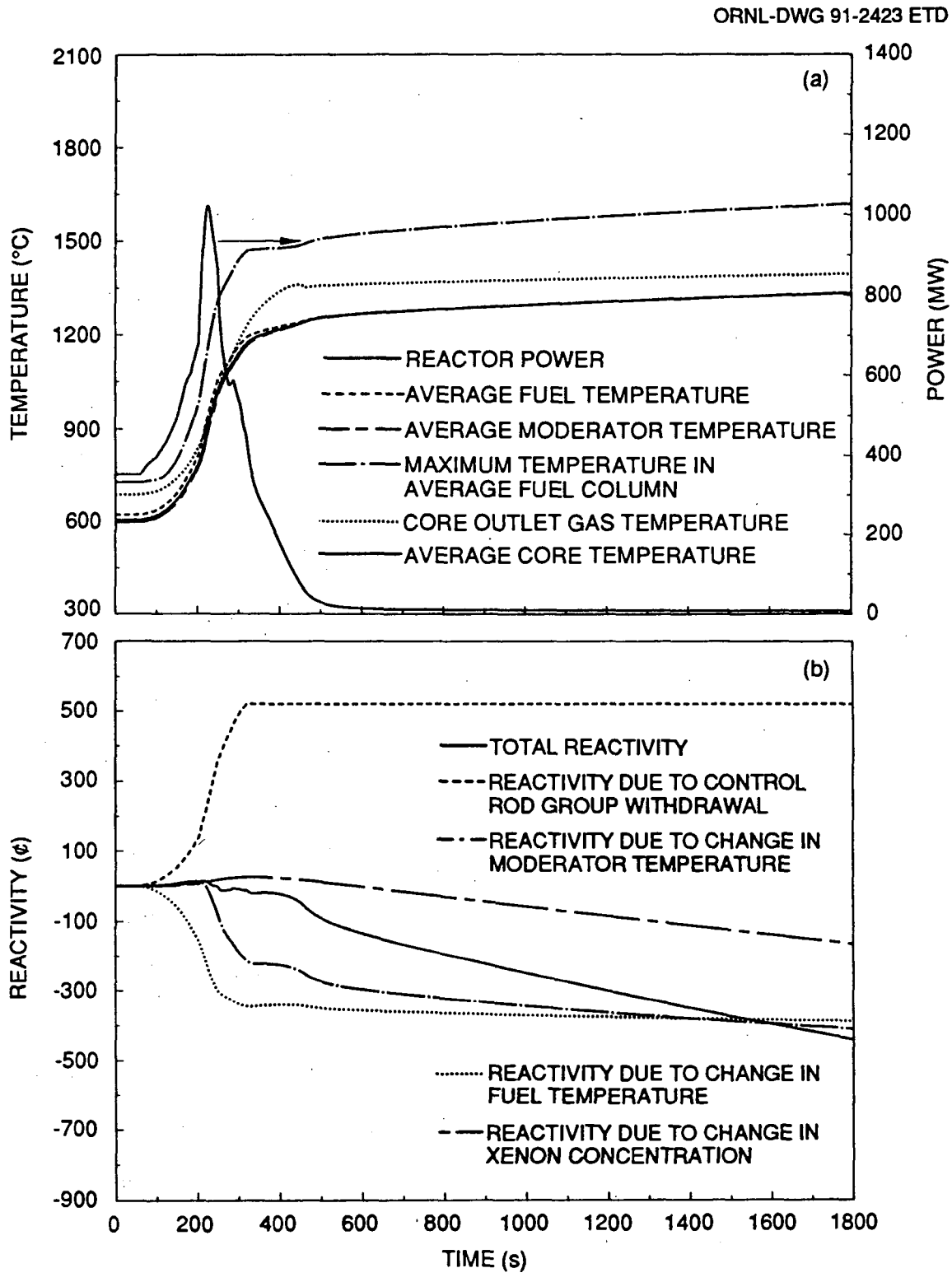

Figure 7.1 ***(a)*** **Temperature and power response during control rod group withdrawal without scram(decreasing core flow);** ***(b)*** **reactivity response during control rod group withdrawal without scram (decreasing core flow)**

8 Examination of Response to Control Rod Group Withdrawal Transient with Scram

8.1 Event Description

Like the cases examined in Sects. 6 and 7, this case involves accidental withdrawal of the highest worth control rod group without action of the neutron flux controller. The reactor scrams on a high power-to-flow ratio. The shutdown cooling system is assumed not to operate. For the time interval analyzed here, this event is similar to SRDC-3 and -4 presented in the PSID.

8.2 Analysis Approach and Assumptions

As in the cases described in Sects. 6 and 7, the worth of the most reactive rod group was taken as 2.5% $\Delta\rho$. The rod group was assumed to be fully inserted initially and to be withdrawn in 260 s. A scram signal is initiated at a neutron flux-to-helium mass flow ratio of 1.5 (selected for conservatism rather than the reference set point of 1.4) using all outer control rods except those being withdrawn accidentally. A scram worth of 9% $\Delta\rho$ was assumed. Based on data from General Atomics,* the delay time from the scram signal until the rods enter the level of the top of the active core was taken as 4.7 s, and the time from the scram signal until the control rods are fully inserted was taken as 23 s. The relation for the relative reactivity introduced vs fraction of insertion for control rod scram was obtained from this communication.*

End-of-equilibrium cycle temperature coefficients and neutron kinetics parameters reported in the PSID were used. The event was analyzed with the model described in Appendix A.

8.3 Results of Control Rod Group Withdrawal Transient with Scram Analyses

Figure 8.1(*a*) and (*b*) show the response of core power, temperatures, and reactivity for the case assuming that the core flow remains constant. For this case, the scram set point for a power-to-flow ratio of 1.5 is reached 78 s after accident initiation (the withdrawal was assumed to begin at t = 60 s). The power peaks at 157% of normal 83 s after accident initiation because nearly 5 s is required before the control rods reach the level of the top of the active core. The average fuel temperature increases only 57°C before beginning to decrease because of the scram.

Figure 8.2(*a*) and (*b*) show the response assuming a reduction in core flow caused by the action of the steam temperature controller. For this case, the scram set point for a power-to-flow ratio of 1.5 is reached 71 s after accident initiation. Because of the decreasing core coolant flow, the power peaks at 128% of normal (at 76 s), and the increase in average fuel temperature is only 45°C.

According to data from General Atomics* the flow signal w used in determining the power-to-flow ratio is obtained by the relation $w \propto (P\Delta P/T_{in})^{0.5}$, where T_{in} is the circulator inlet temperature, P is the system pressure, and ΔP is the pressure rise across the circulator. The T_{in} measuring device has a 20-s time constant, and the pressure measuring device has a 2-s time constant.* Because it would require a system model to accurately compute system pressure and circulator inlet temperature, these delays could not be treated here but should be examined when an overall system simulation, similar to that in Ref. 8, has been prepared. The results presented in the PSID for this event [Design-Basis Event (DBE) No. 4] predict a reactor scram at 99 s after accident initiation, compared with a scram at 71 s for the analyses reported here. Further, the PSID predicts an average fuel temperature increase of 66°C during the rod withdrawal period, compared with an increase in average fuel temperature of 45°C for the analyses reported here.

As time continues beyond the interval analyzed here, cooling would be provided either by the shutdown cooling system, which is not safety related, or by the RCCS, which is safety related.

*J. C. Cleveland, Oak Ridge National Laboratory, personal communication with A. Baxter, General Atomics, June 1987.

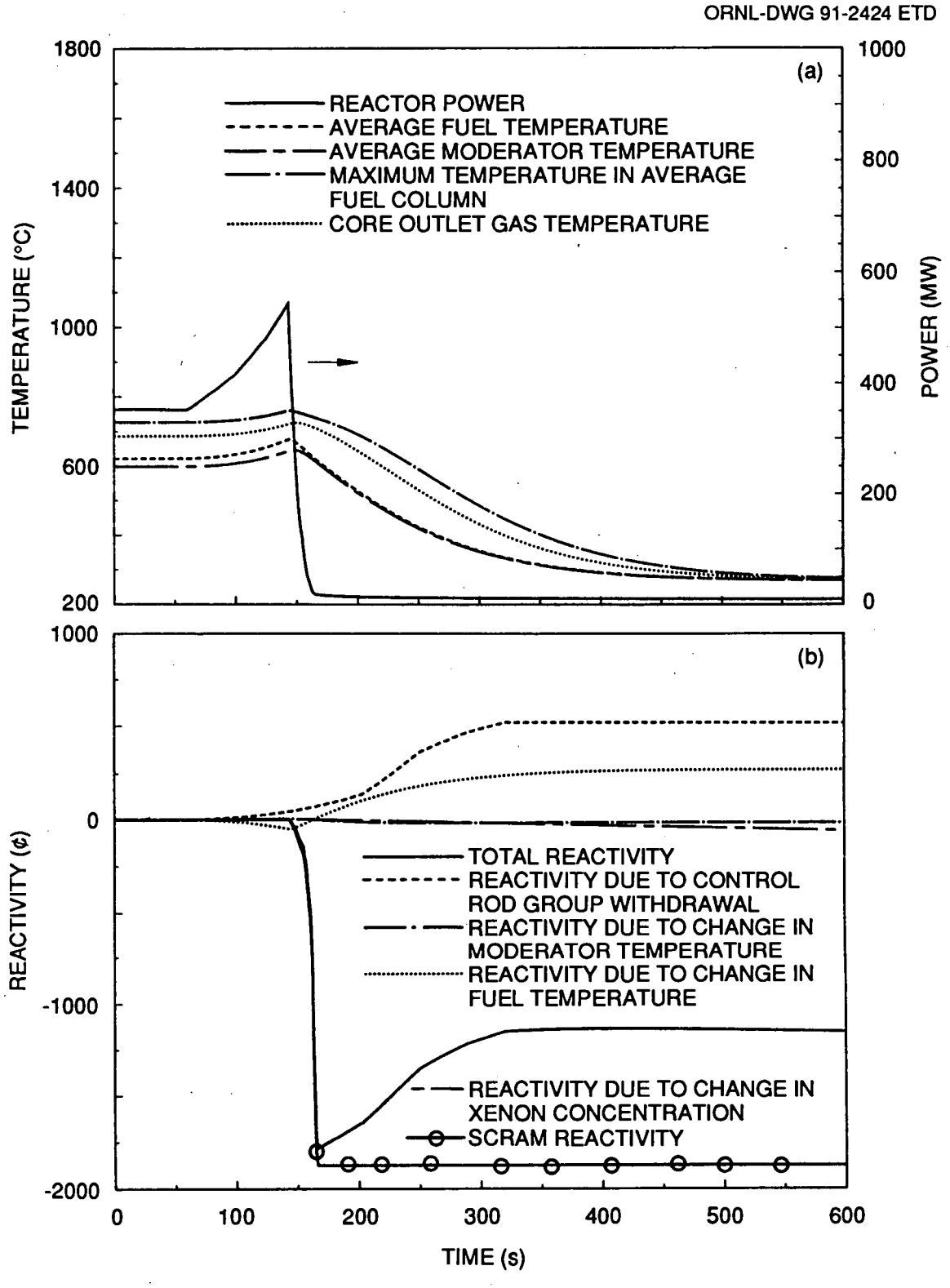

Figure 8.1 *(a)* **Temperature and power response during control rod group withdrawal with scram (constant core flow);** *(b)* **reactivity response during control rod group withdrawal with scram (constant core flow)**

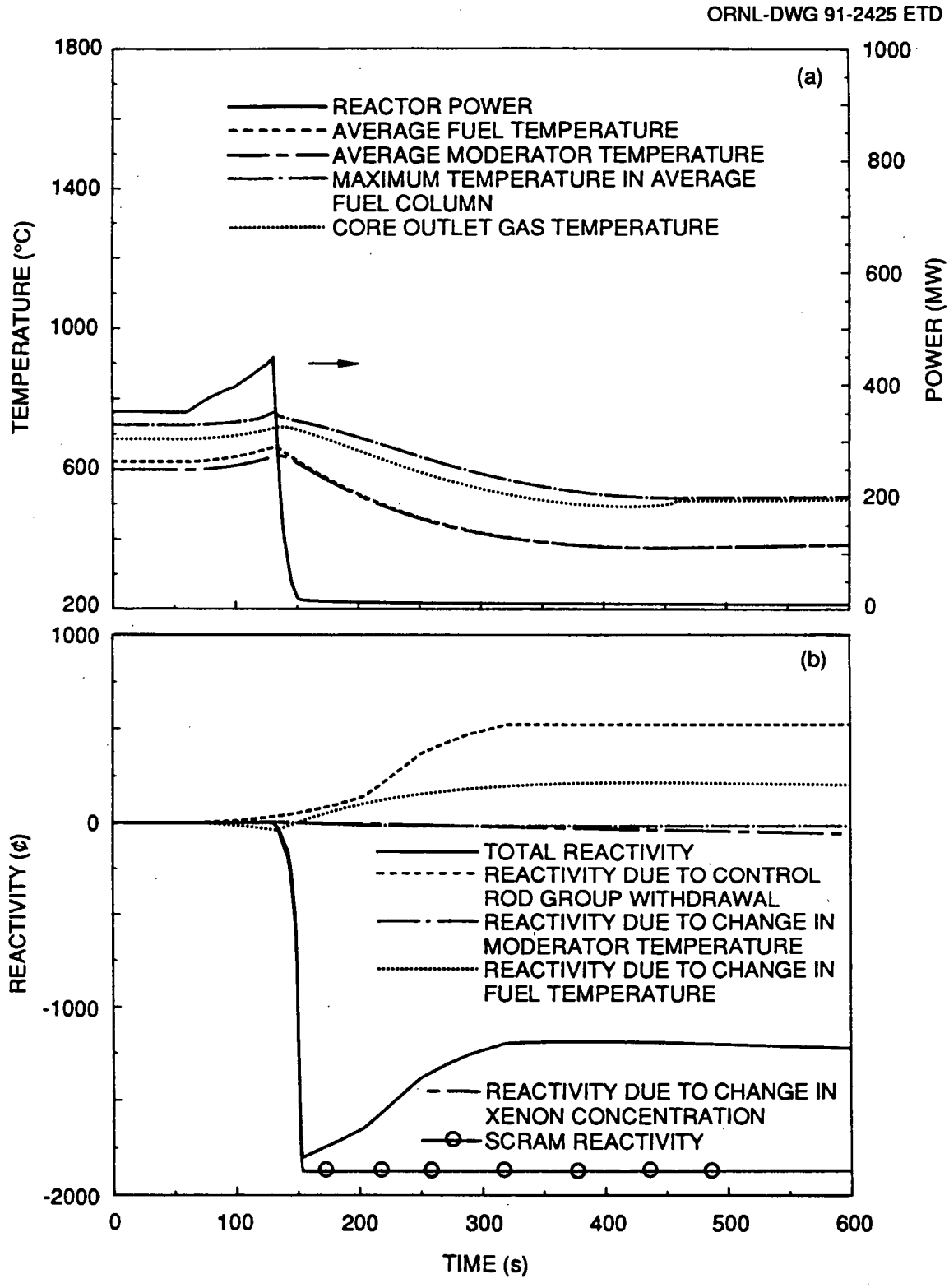

Figure 8.2 ***(a)*** **Temperature and power response during control rod group withdrawal with scram (decreasing core flow);** ***(b)*** **reactivity response during control rod group withdrawal with scram (decreasing core flow)**

9 Examination of Reactor Response to a Rapid Core Cooling Without Scram

9.1 Event Description

This hypothetical event assumes that startup procedures are violated and the reactor is brought to temperatures corresponding to hot full-power operation without coolant flow. The circulators are then started and taken rapidly to full cooling capacity. This results in a rapid cooldown, introducing positive reactivity caused by the negative overall temperature coefficient of reactivity.

This event is examined here because it was identified as a hypothetical method of introducing a large net reactivity (potentially greater than $1.00), which could cause a very rapid and large power excursion that might result in excessive fuel temperatures. The reactor should never be operated in the manner described here.

9.2 Analysis Approach and Assumptions

This case was analyzed using end-of-cycle delayed neutron fractions and temperature coefficients of reactivity with the model described in Appendix A. To investigate the sensitivity of the fuel temperature to the temperature coefficients, a second case was analyzed with the fuel and moderator coefficients each arbitrarily decreased by 2×10^{-5}/°C from its reference value. The initial power level was taken to be 1.0 W, and fuel and moderator temperatures corresponding to full power operation were assumed for initial conditions.

9.3 Results of Rapid Core Cooling Without Scram Analyses

Figure 9.1(*a*) shows the response of core power and temperatures during the rapid cooling event. Figure 9.1(*b*) shows the corresponding response of the core reactivity and its various components. When the helium flow is started and the fuel and moderator begin to cool, the strongly negative fuel temperature coefficient contributes a positive reactivity component. The slightly positive moderator temperature coefficient at normal operating temperatures contributes a negative reactivity component. However, the net reactivity is positive, and the power begins to increase rapidly. Until the power reaches levels that cause significant heating of the core, the net reactivity continues to increase and approaches $1.00. However, the power increase causes heatup of the core, which in turn decreases the net reactivity through the temperature feedback. Although the power reaches a very high level [850 MW(t)], the total energy deposition is not sufficient to increase temperatures above the initial (normal) values. The final condition is a power level of 350 MW(t), as expected.

A second case was run with both the fuel and moderator temperature coefficients arbitrarily made more negative by 2.0×10^{-5}/°C in order to examine the response to a case involving a net reactivity greater than $1.00. Results for this case are shown in Fig. 9.2(*a*) and (*b*). With the arbitrary decrease in temperature coefficients, when the core begins to cool, both the fuel and moderator temperature change contributions to reactivity are positive. As can be seen, for a short time the net reactivity exceeds $1.00, and the reactor is prompt critical. The power peaks at 1475 MW(t) before temperature feedback limits the excursion.

For this second case, the computations show that the net reactivity is above $1.00 from about t = 15.5 s until t = 20.2 s, or for 4.7 s. During this interval, the power increased by a factor of 1.3×10^5 from 0.0086 MW to 1150.0 MW. Figure 9.3 shows the stable reactor period as a function of reactivity, as determined from the in-hour equation. As is shown in this figure, for reactivities ranging from $1.00 ($\rho = 0.0048$) to $1.20 ($\rho = 0.00576$), the stable period ranges from 0.6 to 0.3 s. During the 4.7-s interval when the reactivity exceeded $1.00, a period of 0.4 s would result in a power increase by the factor of 1.3×10^5, as previously noted. Again, although there is a rapid power increase, the energy deposition is not sufficient to cause fuel temperatures to increase above normal values. The final condition is a power level of 350 MW(t). Because the outlet gas temperature remains at or below the normal full power outlet gas temperature, the primary system pressure does not increase above normal operating levels and the primary system relief valves do not open; thus, the system remains pressurized.

An overcooling transient with an initial power level of 100 kW was also simulated. Results are shown in Fig. 9.4(*a*) and (*b*). As expected, the maximum power is somewhat lower than for the case with an initial power of 1 W, and the temperature response is similar.

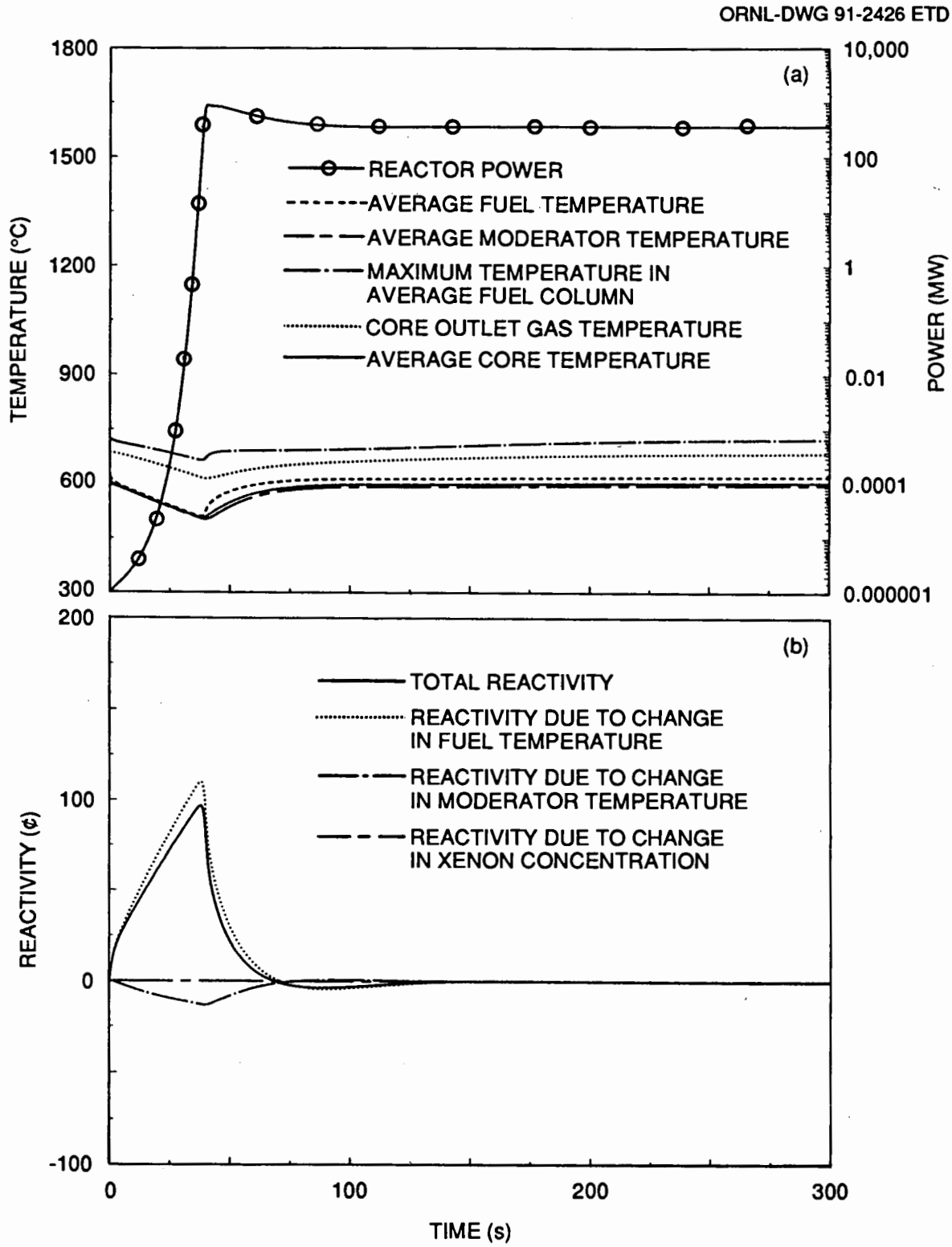

Figure 9.1 *(a)* **Temperature and power response during rapid core cooling event;** *(b)* **reactivity response during rapid core cooling event**

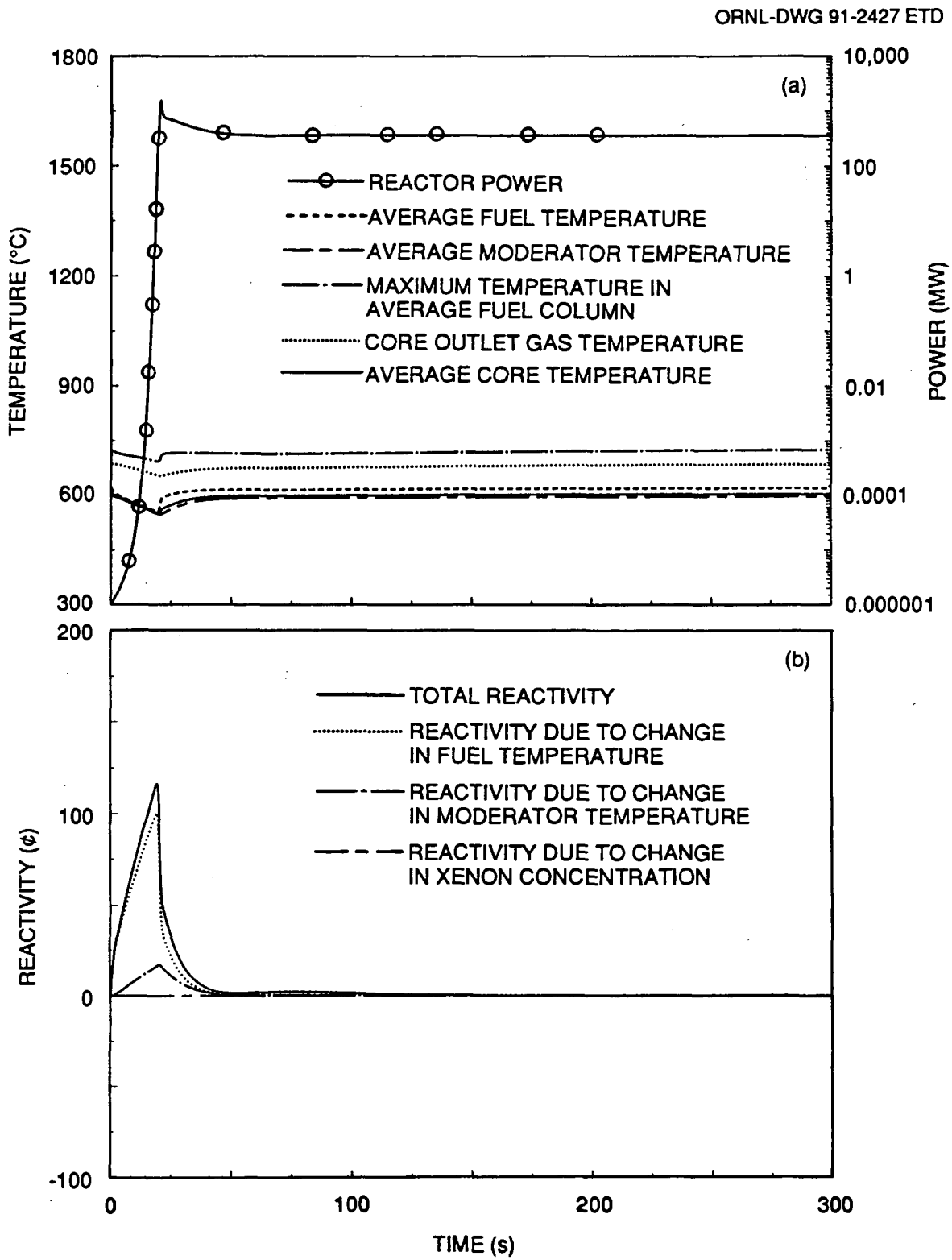

Figure 9.2 *(a)* **Temperature and power response during rapid core cooling event (fuel and moderator temperature coefficient arbitrarily reduced by 2×10^{-5}/°C); *(b)* reactivity response during rapid core cooling event (fuel and moderator temperature coefficients arbitrarily reduced by 2×10^{-5}/°C)**

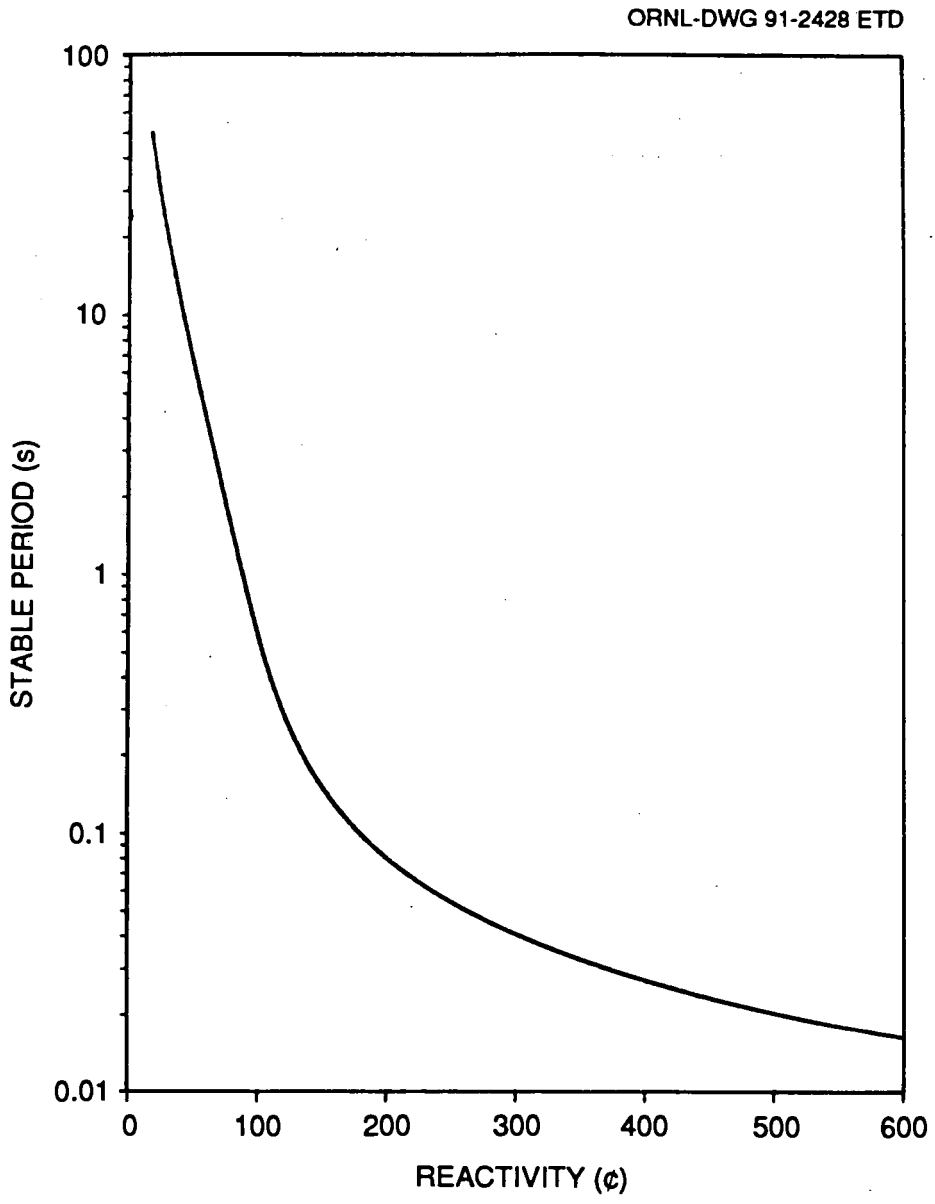

Figure 9.3 Stable period vs reactivity

ORNL-DWG 91-2429 ETD

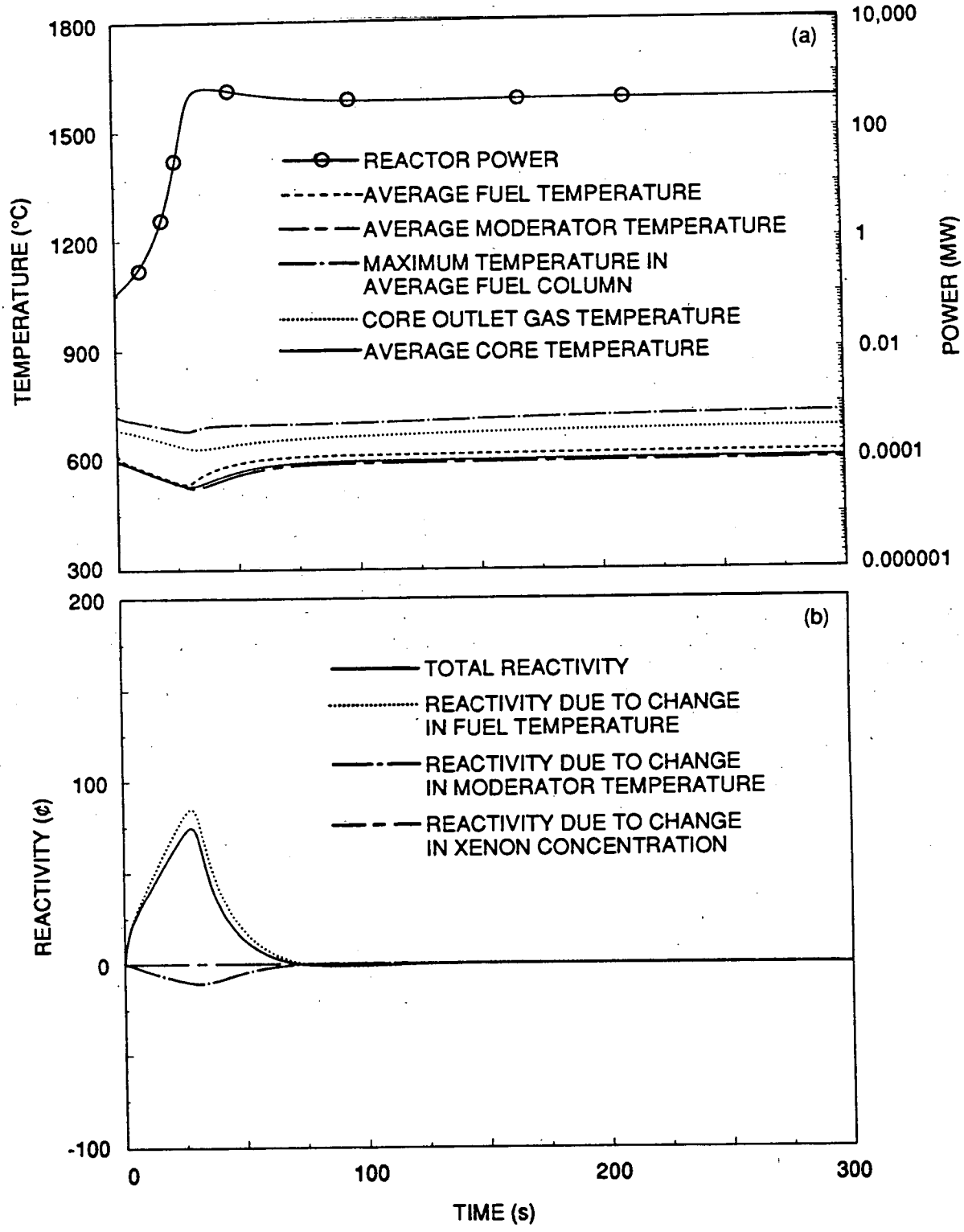

Figure 9.4 *(a)* **Temperature and power response during rapid core cooling event (initial power = 100 kW);** *(b)* **reactivity response during rapid core cooling event (initial power = 100 kW)**

10 Examination of Response to a Control Rod Ejection Transient

10.1 Event Description

This hypothetical event involves rapid ejection of the control rod of highest worth. Although this event is not addressed in the PSID, it is discussed in the probabilistic risk assessment[6] (PRA) to show that fuel temperatures peak well below temperatures that would be expected to cause any significant incremental fuel particle failures. The designers claim that this is a noncredible event because it would require failure of the vessel penetration housing the rod drive and failure of structures located above the housing.[6] In spite of its noncredibility, rod ejection is analyzed here to examine core response to a hypothetical large and rapid reactivity insertion. No scram action or action of the neutron flux controller is considered in this analysis.

10.2 Analysis Approach and Assumptions

For comparison with results presented in the PRA,[6] the same control rod worth (1.1% $\Delta\rho$) and ejection time (10 s) were assumed for these analyses. A second case was analyzed assuming the control rod to be ejected in 1.0 s. (The applicability of the point kinetics model to large and rapid reactivity insertions is discussed in Appendix A.) For both cases, the control rod was assumed to be ejected with the reactor initially at full power. End-of-equilibrium cycle temperature coefficients and neutron kinetics parameters were employed. Because the system would depressurize as a result of the vessel penetration failure, convective heat removal was assumed to cease 5.0 s after initiation of the control rod ejection. The event was analyzed with the model described in Appendix A.

10.3 Results of Control Rod Ejection Analyses

Figure 10.1(*a*) shows the response of the core power and temperatures during the control rod ejection transient with 10 s for the ejection time (the ejection of the control rod is assumed to initiate at t = 5.0 s). Figure 10.1(*b*) shows the corresponding response of the core reactivity and its various components. As is shown in Fig. 10.1(*a*), the power peaks at 15 s (10 s after event initiation) at 3700 MW(t), or at ~10.5 times full power with an increase in average fuel temperature to ~1000°C. The results presented in the PRA[6] predict a power peak of ~2800 MW(t) and an increase of average fuel temperature to ~950°C.

Figure 10.2(*a*) shows the response for the core power and temperatures for the case assuming the rod is ejected in 1.0 s. Figure 10.2(*b*) shows the corresponding response of the core reactivity and its various components. The power peaks at ~4×10^4 MW(t) about 1.0 s after initiation of control rod ejection. The average fuel temperature increases to about 1000°C, which is about 380°C above its initial value. (The nuclear averaged fuel temperature increases by ~480°C.) This maximum power level and the temperature increase can be compared with an approximate analytical prediction of the power and fuel temperature response for large step insertions of reactivity (see Appendix B). For a step reactivity insertion of 1.1% $\Delta\rho$ ($2.29), this approximation predicts a power peak of ~4.3×10^4 MW(t) with a fuel temperature increase of ~360°C.

Although average fuel temperatures remain well below the 1600°C limit for onset of fission product release, this accident must be precluded by the design. Because of neutron flux peaking in the core regions near the rod being ejected, maximum fuel temperatures may not remain within the 1600°C limit.

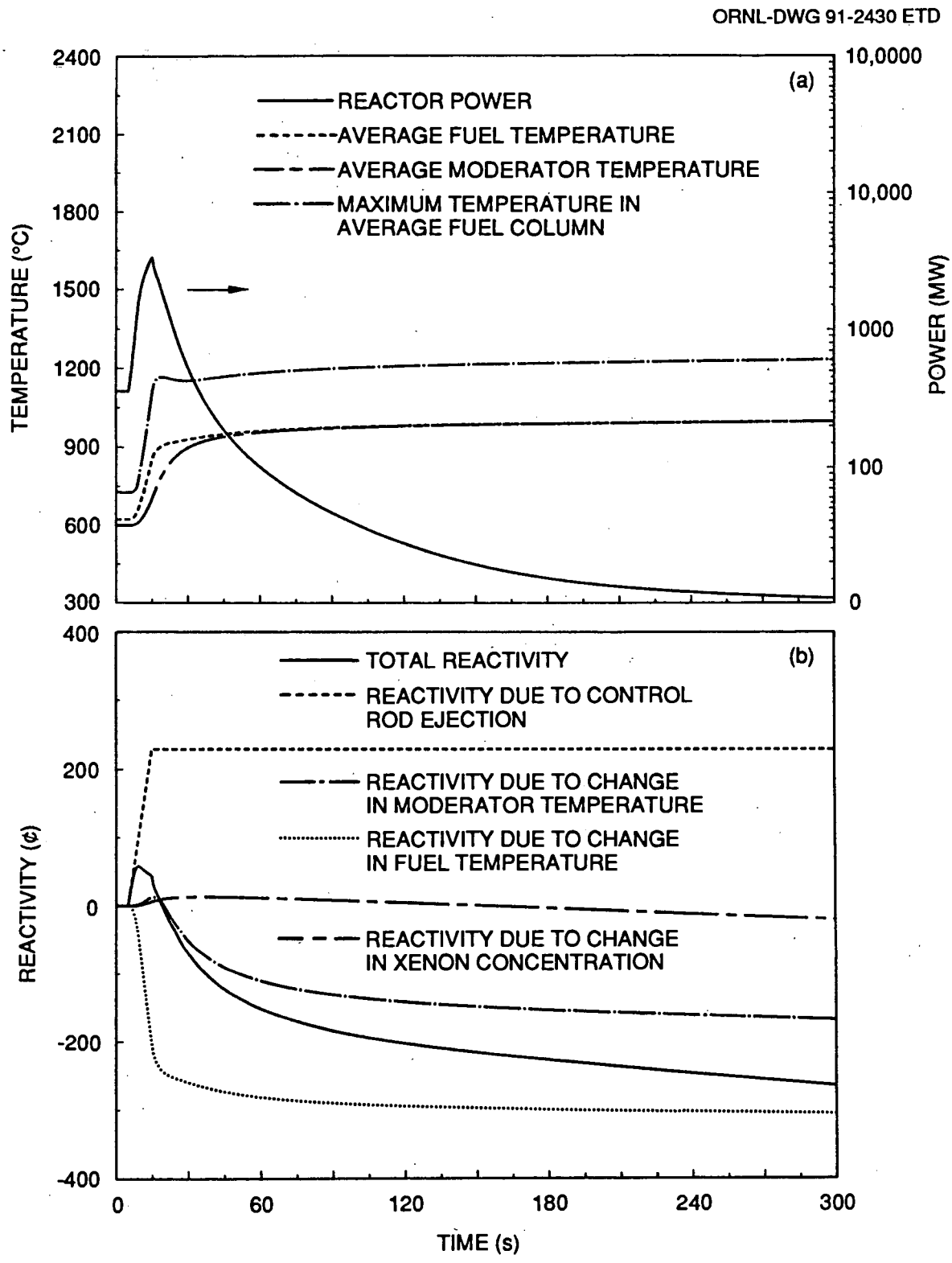

Figure 10.1 *(a)* **Temperature and power response during control rod ejection event (10-s rod ejection time);** *(b)* **reactivity response during control rod ejection event (10-s rod ejection time)**

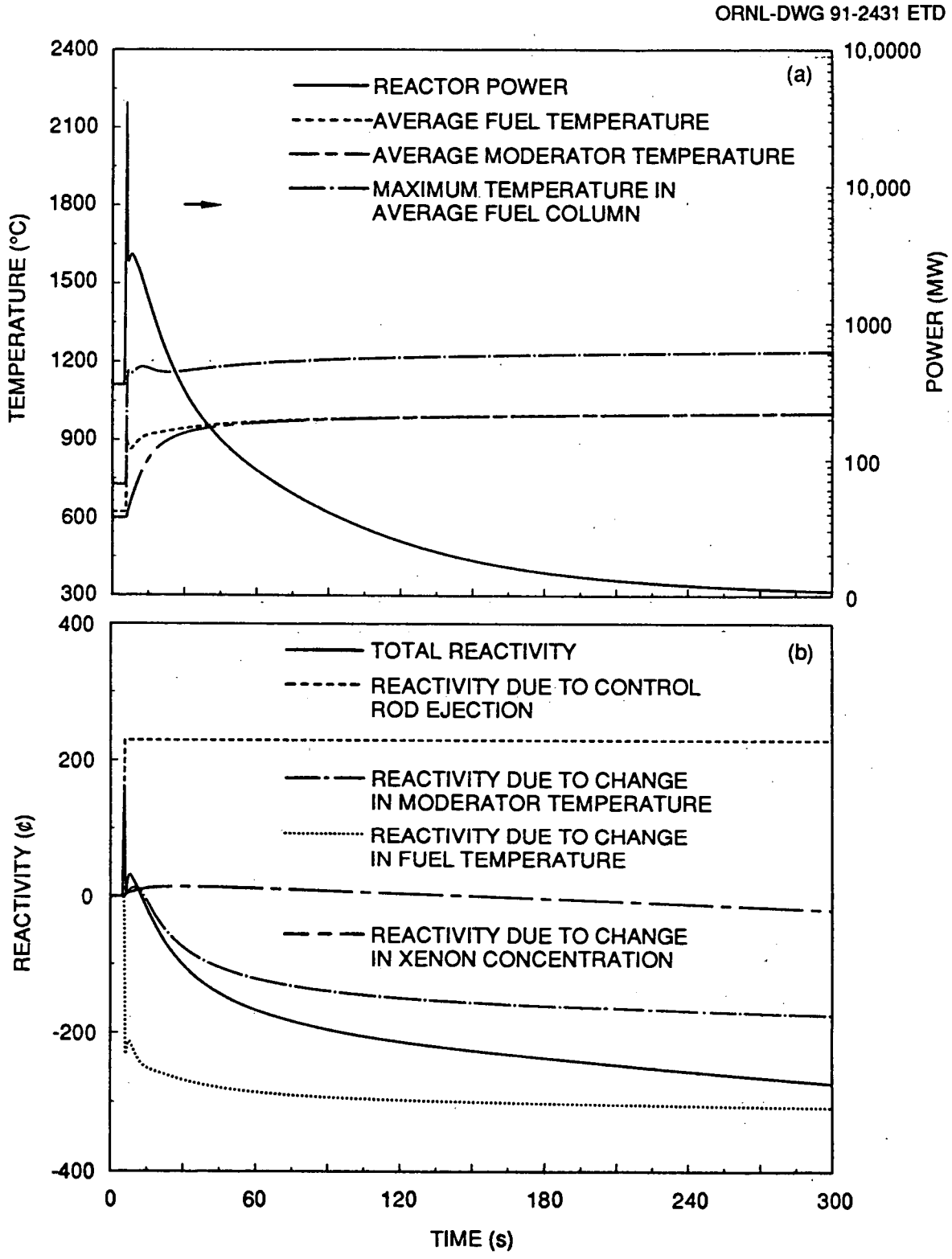

Figure 10.2 *(a)* **Temperature and power response during control rod ejection event (1.0-s rod ejection time);** *(b)* **reactivity response during control rod ejection event (1.0-s rod ejection time)**

11 Examination of Response to a Control Rod Group Ejection Transient

11.1 Event Description

This hypothetical event involves rapid ejection of the control rod group of highest worth. This event is not addressed in the PSID, and the claim is that the design of the plant precludes such an event. The event is analyzed here to investigate the core response to a large and rapid reactivity insertion. No scram action or action of the neutron flux controller is considered in this analysis.

11.2 Analysis Approach and Assumptions

For this event, a reactivity of 2.5% $\Delta\rho$ is assumed to be introduced in 1.0 s. This event was analyzed with the model described in Appendix A. (The applicability of the point kinetics model to large and rapid reactivity insertions is discussed in Appendix A.) End-of-equilibrium-cycle temperature coefficients and neutron kinetics parameters are employed. Because the system would depressurize as a result of the vessel penetration failure, convective heat removal was assumed to cease 5.0 s after initiation of the control rod ejection.

11.3 Results of Control Rod Group Ejection Analyses

Figure 11.1(*a*) shows the response of core power and temperatures during the control rod group ejection transient (the ejection of the control rod group is assumed to initiate at t = 5.0 s). Figure 11.1(*b*) shows the corresponding response of the core reactivity and its various components. As can be seen from Fig. 11.1(*b*), the reactor is prompt critical for nearly 0.5 s (from 5.2 to 5.7 s) with the net reactivity approaching \$2.25 (0.0108 $\Delta\rho$). For such a high reactivity, the corresponding reactor period is 0.065 s, as is shown in Fig. 9.3. The power peaks at 8.1×10^4 MW(t), and the average fuel temperature increases to ~1400°C, which is about 800°C above its initial level. (The nuclear averaged fuel temperature increases about 1000°C above its initial value.) The prompt coefficient is sufficiently negative to terminate the transient; however, as is seen in Fig. 11.1(*a*), fuel temperatures exceed the limit for the onset of fission product release.

The maximum power and the fuel temperature increase just noted can be compared with values predicted by the approximation discussed in Appendix B. For a step reactivity insertion of 2.5% $\Delta\rho$ (\$5.21) the approximation in Appendix B predicts a peak power of about 5×10^5 MW(t) and a fuel temperature increase of about 830°C, which are consistent with the peak power and the fuel temperature increase shown in Fig. 11.1(*a*) and are computed with the model described in Appendix A.

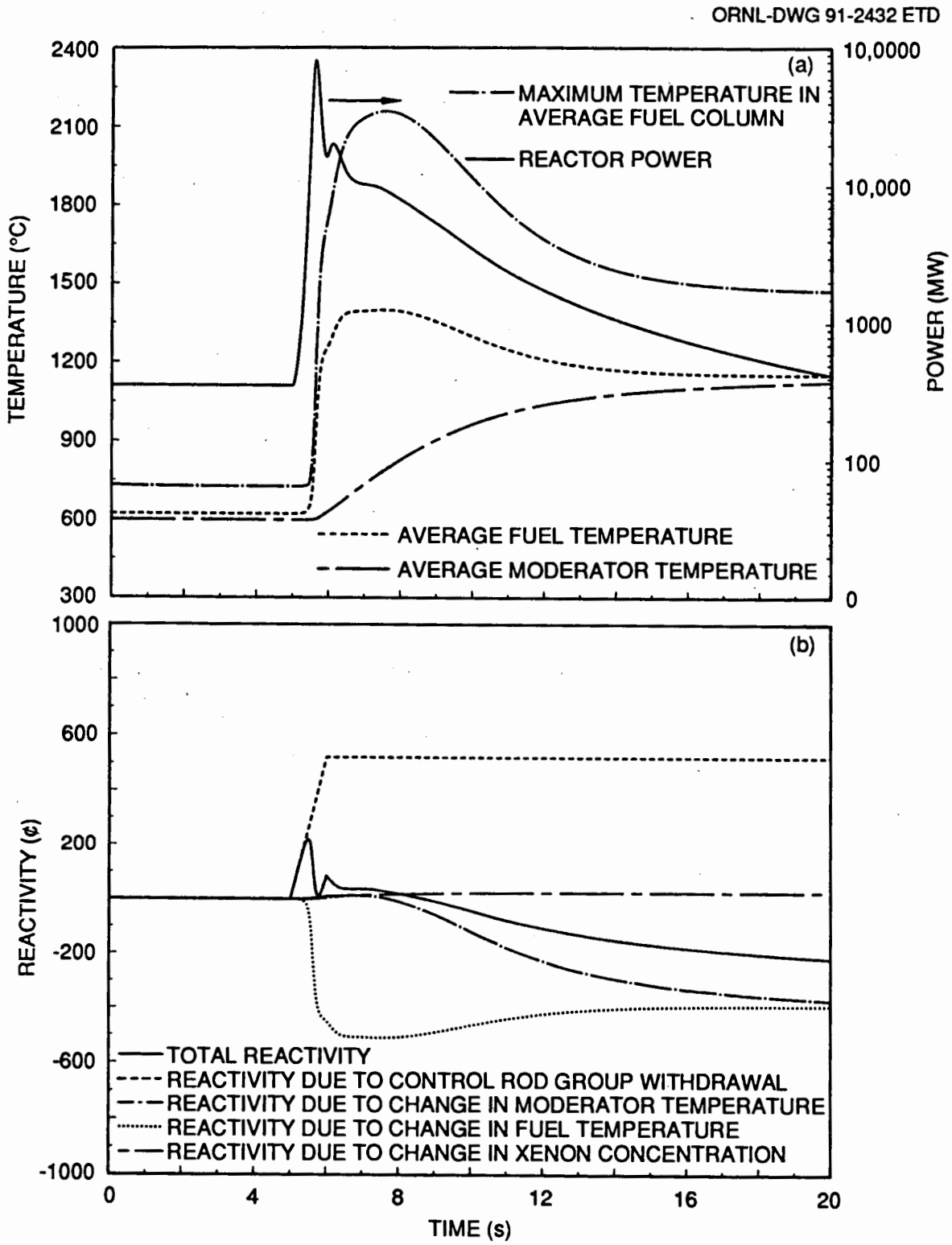

Figure 11.1 *(a)* **Temperature and power response during control rod group ejection event;** *(b)* **reactivity response during control rod group ejection event**

12 Conclusions and Recommendations

Keeping in mind that the designer's values for important neutronic parameters were used, certain conclusions can be drawn. When investigations of the accuracy of these parameters and their uncertainty are complete, certain cases analyzed here should be reexamined.

For events analyzed here, inherent features of the MHTGR design have the potential to provide a high degree of safety. First, there is a large margin of ~500°C between the maximum fuel temperature in normal operation (~1100°C) and the temperature for the onset of fuel failure (~1600°C). Second, the core's high heat capacity and low power density result in slow temperature changes. At full power, the heatup rate of the core with no cooling at all (neither active nor passive)* would be only about 2.7°C/s. At decay power levels, the heatup rate with no cooling at all would be in the range of 1 to 5% of this value. Finally, the negative overall temperature coefficient of reactivity, which is in the range of -2×10^{-5}/°C to -5×10^{-5}/°C, tends to reduce core power as core temperatures increase.

The following general conclusions can be drawn:

1. For events analyzed both here and in the PSID, results of these analyses agree with those presented in the PSID except for the moisture ingress event resulting from the rupture of a single steam generator tube. The reactivity transient resulting from the moisture ingress should be considerably less severe than that reported in the PSID. The PSID analysis for this event was quite conservative because it assumed that water entering the core mainly collects there rather than passing through.
2. No conditions were identified that could lead to transients that are significantly more severe than previously identified. The plant control and protection system scram set points should provide adequate protection for all but control rod or control rod group ejection transients, which should be made impossible by design. Some hypothetical events, if not terminated by reactor scram, could result in temperatures in excess of the 1600°C limit for the onset of fuel failure. However, these events involve combinations of low-probability failures. Further, the 1600°C limit is for longer term heatup, and appropriate limits for short-term power excursion need to be determined.

*This is hypothetical and for illustration only. Clearly, if the core were not cooled it would become subcritical because of the negative temperature feedback and could not remain at full power.

Specific conclusions follow:

1. LOFC:
   - Fuel temperatures should remain below 1600°C if either the control rods or the reserve shutdown material is inserted before recriticality. Several hours are available for this action to be performed.
   - Tests at the AVR pebble bed gas-cooled reactor have shown safe response to a LOFC without scram, including a period of recriticality.
2. Moisture ingress:
   - The reactivity introduced by a single tube rupture does not result in a large power excursion. The transient is fairly slow, and if a scram occurs on a high moisture content or on a high power-to-flow ratio, excessive fuel temperatures will not be reached.
   - The reactor can be driven subcritical by stopping the helium circulator.
3. Control rod group withdrawal transients:
   - Increases in average fuel and moderator temperatures are small if a scram occurs on a high power-to-flow signal.
   - Insertion of control rods or reserve shutdown material is necessary to maintain fuel temperatures below 1600°C.
4. Rapid core cooling event:
   - Fuel temperatures remain well below 1600°C. In fact, fuel temperatures do not rise above normal operating levels. The coupling of core power and temperature through the temperature coefficients of reactivity is such that the resulting temperatures are within acceptable limits.
5. Hypothetical large and rapid positive reactivity insertion:
   - The system should be designed to make large and rapid reactivity insertions incredible.
   - For ejection of a single control rod, core average fuel temperatures remain below 1600°C. However, because of neutron flux peaking in the core regions near the rod being ejected, maximum fuel temperatures may exceed 1600°C.
6. Concerning analysis methods, neglecting the xenon reactivity component is not necessarily conservative because the increased ^{135}Xe burnout rate at the higher than normal neutron flux levels during power excursions adds a positive reactivity component.

Conclusions

The following recommendations are made:

1. Existing fuel-performance data should be examined to determine fuel failure limits for short-term transient overpower events. If relevant fuel behavior data do not exist, fuel performance limits for short-term transient overpower events should be experimentally determined.
2. Analyses similar to those reported here should be performed with an overall system model to properly account for plant control system actions during the transient as well as the response of the steam generator and primary system components. Measurement time constants for various system parameters that are used to initiate scram signals or to affect plant control functions should be considered. These analyses should include consideration of radial peaking factors for the core power and the core flow distribution so that hot-fuel-column analyses can be performed. For events leading to heatup of the steam generator (such as loss of feedwater), tube temperatures should be determined to examine the possibility that the event could lead to tube failure and moisture ingress.
3. The water ingress rate from a single tube rupture reported in the PSID should be independently checked. The rate at which water will adsorb on hot graphite and penetrate into pores in the graphite should be examined and factored into moisture ingress analyses such as those reported here.
4. Investigations should be conducted to determine whether there are mechanisms that could introduce moisture into the core at a higher rate than analyzed here. If larger ingress rates are possible, analyses similar to those reported here should be performed.
5. The long-term response to a control rod group withdrawal accident with scram followed by depressurization (caused by lifting of the primary system relief valve) should be examined. This event is not examined in the PSID, because only a control rod group withdrawal accident with scram followed by a pressurized core heatup is considered (SRDC-3 and DBE-4). However, the results of SRDC-3 and DBE-4 analyses show that the primary system pressure approaches the relief valve set point. Considering the uncertainties in the analyses, and specifically in the computation of system pressure, the depressurized case should also be examined.
6. Independent calculations of parameters such as control rod worth, temperature coefficients of reactivity, and reactivity associated with moisture ingress should be conducted. (Values for these parameters used for the analyses reported here were obtained from the designer.)
7. As questions regarding uncertainties in temperature coefficients and reactivity effects of water are resolved, certain analyses reported here should be repeated if these parameter values are revised in such a way as to result in significantly more severe responses.

References

1. H. Nabielek et al., "The Performance of High-Temperature Reactor Fuel Particles at Extreme Temperatures," *Nuclear Technology* 84, January 1989.*

2. K. J. Krüger and G. P. Ivens, "Safety-Related Experiences with the AVR Reactor," in *Proceedings of a Specialists' Meeting on Safety and Accident Analysis for Gas-Cooled Reactors, Oak Ridge, Tenn., May 13-15, 1985*, IAEA-TECDOC-358, International Atomic Energy Agency.

3. "Ten Years of Electricity Generation with the AVR Pebble Bed Reactor," Arbeitsgemeinschaft Versuchsreaktor AVR GmbH Düsseldorf, Federal Republic of Germany, Dec. 17, 1977.

4. G. Ivens and E. Ziermann, "Safety Aspects of the Operation Experience with the AVR Experimental Power Station," *Proceedings of the Specialists Meeting on Gas-Cooled Reactor Safety and Licensing Aspects*, Lausanne, Switzerland, September 1980.

5. Letter from A. J. Neylan, General Atomics, to T. King, Nuclear Regulatory Comission, Subject: Request for MHTGR Information, dated April 16, 1987.

6. "Probabilistic Risk Assessment for the Standard MHTGR," DOE HTGR-86-011, January 1987.

7. J. C. Cleveland and S. J. Ball et. al. "Simulation of Response of the Fort St. Vrain High-Temperature Gas-Cooled Reactor System to a Postulated Rod Withdrawal Accident," *Proceedings of the ANS Topical Meeting on Thermal Reactor Safety*, Sun Valley, Idaho, July 31-August 4, 1977, ORNL/CONF-770708.†

8. J. C. Cleveland et. al., "ORTAP: A Nuclear Steam Supply System Simulation for the Dynamic Analysis of High-Temperature Gas-Cooled Reactor Transients," USNRC Report, ORNL/NUREG/TM-78, September 1977.†

*Available in public technical libraries.

†Available for purchase from the National Technical Information Service, Springfield, VA 22161.

Appendix A

Description of the Coupled Neutron Kinetics–Core Heat Transfer Dynamics Model

The coupled neutron kinetics–core heat transfer dynamics model was formulated using the techniques for the high-temperature gas-cooled reactor (HTGR) dynamic analyses developed at Oak Ridge National Laboratory (ORNL) during the past 17 years. These techniques have been proven to produce computed results in good agreement with the measured transient response of the Arbeitsgemeinschaft Versuchs Reaktor (AVR) and of the Fort St. Vrain (FSV) reactor. Comparisons of computations with the measured response of the AVR are reported in Ref. A.1, and comparisons of computations with the measured response of the FSV reactor are reported in Ref. A.2. These comparisons have been performed for reactivity insertions of up to ~10¢ at rates up to 2¢/s, as well as for flow reductions including complete loss of forced circulation, with natural convection flow only. Although these reactivity insertions and insertion rates are small compared with some considered in the current analyses, the good agreement of computations with measured response for the FSV reactor and for the AVR provides some confidence that the modeling techniques provide reasonable results.

The importance of space and spectral effects in neutron kinetics calculations for HTGR reactivity accidents has been investigated by R. Brogli and R. Froelich[3] with a multienergy group, one-dimensional kinetics model. Their conclusion is that a point kinetics (one group) model with six groups of delayed neutron precursors, such as the model described in this appendix, is sufficiently accurate for slow reactivity changes such as those resulting from fuel and moderator temperature changes and/or slow rod withdrawal transients (as opposed to rod ejection transients). Based on the maximum control rod group worth presented in the PSID and on the fractional rod worth vs fraction inserted curve, the total reactivity that can be inserted during a control rod group withdrawal accident at full power is no more than $5.20 with a maximum rate of about 4¢/s. The net rate of reactivity insertion is considerably less than 4¢/s if temperature feedback effects are included. However, control rod group ejection accidents would introduce a total reactivity of approximately $5.20 in 1.0 to 10.0 s. Brogli and Froelich found that for the rapid reactivity insertions associated with control rod ejection accidents, the point kinetics model underestimated the peak core power during the transient by ~50% compared to a space and spectral dependent model.

To meet the objective of this study, IBM's Continuous System Modeling Program (CSMP) language was used. CSMP is an application-oriented language that accepts models expressed in the form of ordinary differential equations and/or analog block diagrams. FORTRAN subprograms are generated internally and are output by the CSMP package.

Input to the computational model includes a geometrical description of the core and fuel, the axial flux profile, fuel and moderator thermal properties, delayed neutron parameters, prompt neutron lifetime, ^{135}Xe reactivity worth, ^{135}Xe microscopic absorption cross section, core macroscopic fission cross section, total neutron flux, and fuel and moderator temperature coefficients of reactivity. The time dependence of the reactivity introduced by control rod motion is also required as input.

Core Neutronics Model

To determine the core neutronic response, the model employs the point kinetics equations with six groups of delayed neutron precursors:

$$\frac{dC_i}{dt} = -\lambda_i \; C_i + \frac{\beta_i}{\Lambda} P \quad i = 1, \ldots, 6 , \qquad \text{(A.1a)}$$

and

$$\frac{dP}{dt} = \frac{\rho - \beta_T}{\Lambda} P + \sum \lambda_i C_i , \qquad \text{(A.1b)}$$

where

C_i = delayed neutron precursor concentration for group i,
λ_i = delayed neutron decay constant (s^{-1}) for group i,
β_i = delayed neutron fraction for group i,
ρ = reactivity [=(k – 1)/k],
P = reactor power, fraction of full power,
$\beta_T = \Sigma \beta_i$,
Λ = prompt neutron generation time (assumed constant).

The six delayed neutron decay constants (λ_i) and delayed neutron fractions (β_i) were based on information in Ref. A.4. The values of the six delayed neutron yield fractions (β_i) were obtained for end-of-equilibrium cycle conditions as the weighted average of the delayed neutron fractions for each group of delayed neutrons for ^{233}U, ^{235}U, and

^{239}Pu using the relative fission rates (obtained from General Atomics*) as the weighting factors.

The resulting values of λ_i and β_i for end-of-equilibrium cycle conditions are given in Table A-1. These give a value for $\beta_T = 0.0048$. The value used for the neutron reproduction time was 0.4 ms, which was obtained from Ref. A.5.

Table A-1 Delayed neutron precursor data

Delayed neutron group	β_i	$\lambda_i(s^{-1})$
1	0.00017	0.012375
2	0.00113	0.03013
3	0.000974	0.11177
4	0.00183	0.30130
5	0.00052	1.13607
6	0.00020	3.0130

Temperature Feedback and Xenon Reactivity Models

The time-dependent reactivity changes caused by changing fuel and moderator temperatures are determined from

$$\Delta\rho_f(t) = \int_{\overline{T}_{f,ref}}^{\overline{T}_f} \alpha_f(T)dT \ , \qquad (A.2a)$$

and

$$\Delta\rho_m(t) = \int_{\overline{T}_{m,ref}}^{\overline{T}_m} \alpha_m(T)dT \ , \qquad (A.2b)$$

where α_f and α_m are the fuel and moderator temperature coefficients of reactivity, respectively; and

$\overline{T}$ ≡ nuclear average (fuel or moderator) temperature

$$\equiv \sum \phi_i^2 \ v_i \ T_i / \left(\sum \phi_i^2\right) , \qquad (A.3)$$

where T_i is the (fuel or moderator) temperature in the *i*th axial segment of the core as computed by the heat transport model, ϕ_i^2 is the flux-squared importance weighting, and v_i is the nodal volume fraction. The temperature coefficients were treated as temperature dependent.

Although the calculational model assumes the fuel temperature coefficient of reactivity to be associated with temperature changes in the entire fuel compact matrix, it is in reality determined by temperature changes in the fuel particles only. To ignore the particle time constant is always conservative in computing the power excursion because doing so delays the negative effect of the fuel temperature increase.

The reactivity worth of the equilibrium ^{135}Xe concentration at steady-state, full-power conditions is 3.2% $\Delta\rho$.† The time-dependent reactivity, $\Delta\rho_{Xe}(t)$, introduced by the changing ^{135}Xe concentration, is computed by

$$\Delta\rho_{Xe}(t) = \Delta\rho_{Xe}(t=0)\left[\frac{X(t)}{X(0)} - 1\right] , \qquad (A.4a)$$

where $\Delta\rho_{Xe}(t = 0) = 0.032$ at full-power steady-state conditions, and X(t) is the ^{135} Xe concentration at time t.

During transients, the time-dependent ^{135} Xe concentration used in Eq. (A.4a) is computed from the following differential equations for ^{135}I and ^{135}Xe concentrations:

$$\frac{dI}{dt} = -\lambda_I I - \sigma_I \phi I + \gamma_I \Sigma_f \phi \ , \qquad (A.4b)$$

and

$$\frac{dX}{dt} = -\lambda_x X - \sigma_x \phi X + \lambda_I I + \gamma_x \Sigma_f \phi \ , \qquad (A.4c)$$

where

- I = ^{135}I concentration,
- X = ^{135}Xe concentration,
- λ = radioactive decay constant,
- σ = one-group microscopic absorption cross section,
- γ = fission yield,
- Σ_f = macroscopic one-group fission cross section of the fuel,
- ϕ = the one-group neutron flux.

The term $\sigma_I \phi I$ is neglected in the equation for ^{135}I concentration because σ_I is less than 0.1 barn, making this term small compared to the others. Values for $\sigma_a(Xe)$ and for the neutron flux ϕ at full power were obtained from General Atomics† as $\sigma_a(Xe) = 1.2 \times 10^6$ barns and $\phi = 1.88 \times 10^{14}$ neutrons/cm^2 s. The value for Σ_f was computed from $P = \kappa \Sigma_f \phi V$ to be $\Sigma_f = 9.81 \times 10^{-4}$ cm^{-1} (κ represents the energy per fission).

The following values were used for the fission yields and radioactive decay constants of ^{135}I and ^{135}Xe (from Ref. A.6):

*D. L. Moses, Oak Ridge National Laboratory, personal communications with A. Baxter, General Atomics.

†A. Baxter, General Atomics, personal communication with J. C. Cleveland, Oak Ridge National Laboratory, June 1987.

$$\gamma_I = 0.061 ,$$

$$\gamma_X = 0.003 ,$$

$$\lambda_I = 2.87 \times 10^{-5}/s , \text{ and}$$

$$\lambda_X = 2.09 \times 10^{-5}/s .$$

The total core reactivity at any time t is then computed from

$$\rho = \Delta\rho_f + \Delta\rho_m + \Delta\rho_{Xe} + \Delta\rho_{\text{control rods}} + \Delta\rho_{\text{moisture}} \quad (A.5)$$

and is used in the point kinetics equation.

After the reactor is driven subcritical, either by the temperature increase or by insertion of control material, the total power including the decay power contribution is computed as the output of a series of optimized lead-lag filters with prompt power as an input and with filter coefficients and time constants selected to match decay power generation following a step decrease in flux to zero. The relation for decay power vs time from fission products was obtained from Ref. A.7 as

$$\frac{P(t)}{P(t=0)} = At^{-a} , \quad (A.6)$$

with

t = time after shutdown in seconds

and with

A = 0.0603 and a = 0.0639 for $0 < t < 10$ s ,

A = 0.0766 and a = 0.181 for $10 < t < 150$ s , and

A = 0.13 and a = 0.283 for $150 < t < 4 \times 10^6$ s.

In obtaining the above relationship, an infinite irradiation time was assumed.

Core Heat Transfer Model

The core is composed basically of an array of triangular cells as shown in Fig. A.1(a). The coupled neutron kinetics-heat transfer model determines the axial profile of fuel, moderator, and coolant temperatures along a representative unit cell containing an average fuel stick, that is, a fuel stick with a radial relative power density factor of 1.0. The axial power profile was obtained from Ref. A.8. For conditions for which the heat conduction to or from the average triangular cell is negligible compared to the difference between the heat generated and the heat removed by the coolant from the cell, the three lateral surfaces of the average triangular unit cell can be modeled as surfaces of zero heat flux. The temperature feedback components of the core reactivity are determined based on changes in the average fuel and moderator temperatures within this unit cell.

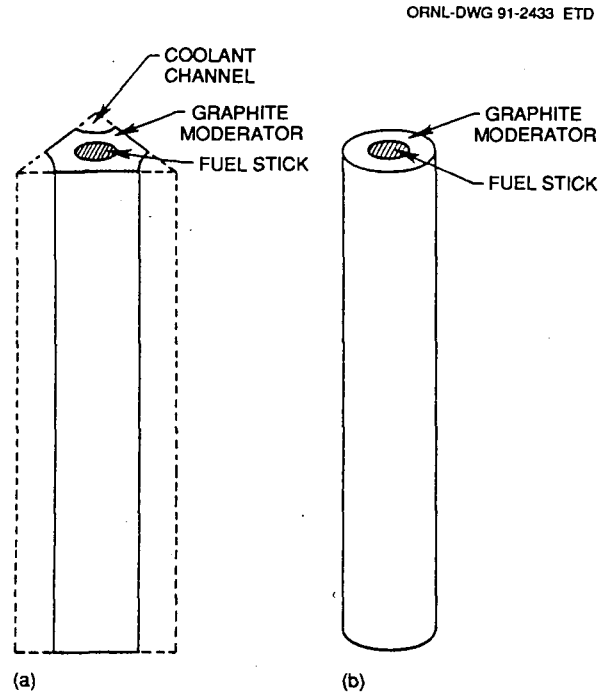

Figure A.1 ***(a)* Basic triangular cell of MHTGR fuel block; *(b)* equivalent cylindrical cell**

For calculational purposes, the three-dimensional average triangular cell [Fig. A.1(*a*)] is converted to an equivalent two-dimensional (r-z) cylindrical cell, as shown in Fig. A.1(*b*). This equivalent cell consists of a fuel stick surrounded by an annular ring of moderator that is cooled by helium flow. The heat conduction equations can then be solved in two-dimensional geometry rather than three-dimensional geometry. The following modeling techniques are used to ensure that the equivalent cylindrical cell representation adequately models the dynamic response of the three-dimensional triangular element:

1. Because of the importance of the moderator heat capacity in transient calculations, the heat capacity of the moderator in the triangular element is conserved in transforming to the cylindrical cell.
2. The actual moderator-to-coolant heat transfer area in the triangular element is used in determining the area for convective heat transport.
3. The moderator thermal conductance in the cylindrical model is modified by dividing by a "shape factor" to account for the change from the moderator's actual geometry. The intent of this shape factor is to force the temperature drop across the moderator as calculated by the cylindrical model to agree with the difference between the average moderator temperatures at the surfaces of the fuel holes and the coolant holes,

respectively, as would be calculated by a detailed three-dimensional representation. Based on previous HTGR analyses (Ref. A.9) in which steady-state and transient calculations for a two-dimensional cell were compared with detailed three-dimensional calculations, a value of 2.2 was selected for the shape factor.

To determine the steady-state and transient temperatures, a lumped node model of the average fuel/moderator column in the core is employed. This average column is modeled by 20 axial sections. It is assumed that heat transfer by conduction in the solid in the axial direction is negligible compared to the heat conducted outward from the fuel through the moderator and taken up by the coolant gas. This tends to be a fairly accurate as well as somewhat conservative assumption. Therefore, the calculation of heat transfer in the solid becomes a set of radial heat transfer calculations coupled axially by means of the flowing coolant gas. The core inlet flow rate and inlet temperature can be varied during the transient by input.

Each of the 20 axial sections representing an average fuel/moderator column contains 3 nodes. Two of these nodes represent radial sections of the fuel stick, and one node represents the moderator. Therefore, the transient thermal response is modeled by 60 first-order, nonlinear, time-dependent ordinary differential equations. This results in the following equations for the temperatures in the fuel stick and surrounding moderator in each axial section of the cylindrical unit cell:

$$\frac{d\overline{T}_{f1}}{dt} = \frac{\dot{Q}_{f2}V_{f1}}{(Mc_p)_{f1}} + \frac{C_1}{(Mc_p)_{f1}}\left(\overline{T}_{f2} - \overline{T}_{f1}\right) , \quad \text{(A.7a)}$$

$$\frac{d\overline{T}_{f2}}{dt} = \frac{\dot{Q}_{f2}V_{f2}}{(Mc_p)_{f2}} + \frac{C_1}{(Mc_p)_{f2}}\left(\overline{T}_{f1} - \overline{T}_{f2}\right) + \frac{C_2}{(Mc_p)_{f2}}\left(\overline{T}_m - \overline{T}_{f2}\right) , \quad \text{(A.7b)}$$

and

$$\frac{d\overline{T}_m}{dt} = \frac{\dot{Q}_m V_m}{(Mc_p)_m} + \frac{C_2}{(Mc_p)_m}\left(\overline{T}_{f2} - \overline{T}_m\right) + \frac{C_3}{(Mc_p)_m}\left(\overline{T}_3 - \overline{T}_m\right) , \quad \text{(A.7c)}$$

where

$\overline{T}_{f1}$ = average temperature in the inner node of the fuel stick in the axial section of the unit cell (the inner node represents the fuel stick mass from $r = 0$ to $r = r_i$ where $r_i < R_f$; R_f is the radius of the fuel stick),

$\overline{T}_{f2}$ = average temperature in the outer node of the fuel stick in the axial section of the unit cell,

$\overline{T}_m$ = average moderator node temperature in the axial section of the unit cell,

$\overline{T}_s$ = average moderator temperature at the surface of the coolant channels in the axial section of the unit cell,

$\dot{Q}_m$ = time-dependent power generation per unit volume in the moderator

$\dot{Q}_f$ = time-dependent power generation per unit volume in the fuel stick,

M = mass,

V = volume,

c_p = specific heat,

C_1 = thermal conductance from the inner fuel stick node to the outer fuel stick node,

C_2 = thermal conductance from the outer fuel stick node to the moderator node,

C_3 = thermal conductance from the moderator node to the surface of neighboring coolant channels,

To obtain the correct lumped node temperatures at steady state, it is necessary to derive the conductances C_1, C_2, and C_3 so that the terms $C_1(\overline{T}_{f1} - \overline{T}_{f2})$, $C_2(\overline{T}_{f2} - \overline{T}_m)$, and $C_3(\overline{T}_m - \overline{T}_s)$ properly represent the heat flow between successive radial nodes. This is done using the steady-state radial temperature profiles in the cylindrical unit cell. In deriving these conductances, all of the heat is assumed to be generated uniformly in the fuel stick. With that assumption, the temperature profile in the fuel stick is parabolic, and the temperature profile in the annular ring representing the moderator is logarithmic, that is,

$$T(r) = T(r=0) - \frac{\dot{Q}_f}{4k_f} r^2 \quad \text{for } r \le R_f , \quad \text{(A.8a)}$$

and

$$T(r) = T(R_{im}) - \frac{\dot{Q}_f R_f^2}{2k_{m,eq}} \ln\left(r/R_{im}\right) \quad \text{for } R_{im} < r < R_{om} , \quad \text{(A.8b)}$$

where

$\dot{Q}_f$ = the power generation in the fuel stick per unit volume (assumed uniform in the radial dimension),

k_f = thermal conductivity of the fuel stick,

$k_{m,eq}$ = equivalent thermal conductivity of the moderator = k_m/s, where s is the shape factor,

R_{im} = radius of the fuel hole in the graphite block,

R_{om} = radius of the annular ring of moderator in the unit cell,

R_f = radius of the fuel stick.

In the unit cell, for steady-state conditions, the heat flow between the inner fuel stick node (representing the fuel stick mass from $r = 0$ to $r = r_i$) to the outer fuel stick node (representing the fuel stick mass from $r = r_i$ to $r = R_f$) is $\dot{Q}_f V_{f1}$. Conductance between these nodes is therefore obtained from

$$C_1 = \dot{Q}_f \pi \Delta z r_i^2 / \left[\overline{T}_{f1} - \overline{T}_{f2}\right] , \qquad (A.9a)$$

where Δz is the axial length of the unit cell,

$$\overline{T}_{f1} = \frac{1}{\pi \Delta z r_i^2} \int_0^{r_i} T(r)\ dV , \qquad (A.9b)$$

and

$$\overline{T}_{f2} = \frac{1}{\pi \Delta z \left(R_f^2 - r_i^2\right)} \int_{r_i}^{R_f} T(r)\ dV . \qquad (A.9c)$$

Performing the integrations to obtain $\overline{T}_{f1}$ and $\overline{T}_{f2}$ and using the results to obtain C_1 from Eq. (A.9a) gives

$$C_1 = 8\pi k_f \Delta z (r_i / R_f)^2 . \qquad (A.10)$$

To derive C_2, note that in the unit cell, for steady state, the heat flow from the outer fuel stick node to the moderator node is $\dot{Q}_f V_f$, where V_f is the volume of the fuel stick in the unit cell. Therefore, C_2 is obtained so that $\dot{Q}_f V_f = C_2(\overline{T}_{f2} - \overline{T}_m)$.

The total conductance C_2 is related to the individual conductances from the fuel node to the moderator node by

$$\frac{1}{C_2} = \frac{1}{C_A} + \frac{1}{C_{gap}} + \frac{1}{C_B} , \qquad (A.11a)$$

where

$$C_A = \dot{Q}_f V_f / \left[\overline{T}_{f2} - T(R_f)\right] , \qquad (A.11b)$$

$$C_{gap} = \dot{Q}_f V_f / \left[T(R_f) - T(R_{im})\right] , \qquad (A.11c)$$

$$C_B = \dot{Q}_f V_f / \left[T(R_{im}) - \overline{T}_m\right] , \qquad (A.11d)$$

and

$$\overline{T}_{f2} = \frac{1}{\Delta z \pi \left[R_f^2 - r_i^2\right]} \int_{r_i}^{R_f} T(r)\ dV , \qquad (A.11e)$$

$$\overline{T}_m = \frac{1}{V_m} \int_{r_{im}}^{R_{om}} T(r)\ dV . \qquad (A.11f)$$

(Note that with these definitions,

$$\left(\frac{1}{C_A} \frac{1}{C_{gap}} \frac{1}{C_B}\right)^{-1} = \left[\frac{\overline{T}_{f2} - T(R_f)}{\dot{Q}_f V_f} + \frac{T(R_f) - T(R_{im})}{\dot{Q}_f V_f} + \frac{T(R_{im}) - \overline{T}_m}{\dot{Q}_f V_f}\right]^{-1} = \frac{\dot{Q}_f V_f}{\left(\overline{T}_{f2} - \overline{T}_m\right)} , \qquad (A.11g)$$

as desired.)

Performing the integrations to obtain $\overline{T}_{f2}$ and $\overline{T}_m$ and using the results to obtain C_A and C_B gives

$$C_A = 8\pi k_f \Delta z \left[1.0 - (r_i R_f)^2\right] , \qquad (A.12a)$$

and

$$C_B = \frac{\pi \Delta z\ k_{m,eq}}{\left[\dfrac{R_{om}^2 \ln(R_{om} / R_{im})}{2\,(R_{om}^2 - R_{im}^2)} - \dfrac{1}{4}\right]} . \qquad (A.12b)$$

These values of C_A, C_B, and C_{gap} are then substituted into Eq. (A.11a) to obtain C_2. Similarly, $C_3 = \dot{Q}_f V_f / [T_m - \overline{T}(R_{om})]$, and after substituting for $\overline{T}_m$ and $T(R_{om})$,

$$C_B = \frac{\pi \Delta z\ k_{m,eq}}{\left[\dfrac{\ln(R_{om} / R_{im})}{2} - \dfrac{R_{om}^2 \ln(R_{om} / R_{im})}{2\,(R_{om}^2 - R_{im}^2)} + \dfrac{1}{4}\right]} . \qquad (A.13)$$

The gas temperature in each of the 20 axial sections of the core is computed from the inlet temperature, T_{in}, to that axial section and the coolant channel surface temperature, T_s, in that axial section according to the "exponential approach" technique (Ref. A.9):

$$T_{gas}(z) = e^{-nz/L}\ T_{in} + \left(1 - e^{-nz/L}\right) T_s , \qquad (A.14a)$$

where

$n = \dfrac{hA}{WC_{p,he}}$ (a dimensionless "section length"),

W = helium mass flow rate through coolant channel,

$C_{p,he}$ = helium specific heat (5195 J/kg K),

h = heat transfer coefficient,

L = length of the axial section,

A = total coolant channel surface area in axial section of core.

This relation is the exact solution to the equation

$$WC_{p,he}\ dT_{gas}(z) = h[T_s - T_{gas}(z)]dA\ , \qquad (A.14b)$$

where T_s is assumed constant in the axial direction within the section (an approximation that becomes more accurate as the number of axial sections used in the model increases). Therefore, the gas outlet temperature from each axial section is

$$T_{out} = e^{-n}\ T_{in} + (1 - e^{-n})T_s\ . \qquad (A.15)$$

The surface temperature, T_s, of the moderator cell in each axial section is derived by equating the heat flowing from the moderator to the coolant channel surface with the heat removal by convection; that is

$$C_3(\overline{T}_m - T_s) = hA\ (T_s - \overline{T}_{gas})\ , \qquad (A.16)$$

where $\overline{T}_{gas}$ is the average gas temperature in the axial segment of the core.

Defining $\tau_F = \dfrac{hA}{C_3}$, this gives

$$T_s = \left(\overline{T}_m + \tau_F \overline{T}_{gas}\right)\Big/(1 + \tau_F)\ . \qquad (A.17)$$

Integrating Eq. (A.14a) over an axial section gives

$$\overline{T}_{gas} = T_s + \frac{1}{n}(e^{-n} - 1)(T_s - T_{in})\ , \qquad (A.18)$$

so

$$T_s = \left[\frac{\overline{T}_m}{1+\tau_F} - \frac{\tau_F}{1+\tau_F}\frac{1}{n}\left(e^{-n} - 1\right)T_{in}\right]\Bigg/$$

$$\left\{1 - \frac{\tau_F}{(1+\tau_F)}\left[1 + \frac{1}{n}\left(e^{-n} - 1\right)\right]\right\}\ . \qquad (A.19)$$

The quasi-static approximation for gas temperature [Eq. (A.18)] is practical because of the very small energy storage in the helium relative to that in the solid materials in the core and because of the very short transport time of helium through the core relative, for example, to the thermal time constant of the fuel. (This approximation is investigated in detail in Ref. A.10.) Thus, helium temperature is coupled algebraically to the solid temperature (rather than via a first-order time-dependent differential equation). The solid temperatures are, of course, calculated from coupled, first-order, nonlinear differential equations [Eqs. (A.7a), (A.7b), and (A.7c)].

The heat transfer coefficient from the coolant channel surface to the coolant is computed with the following correlation from Ref. A.11:

$$Nu = (0.02)\ Re^{0.8}\ , \qquad (A.20)$$

with

$$Re = \frac{(\dot{m}/A)d}{\eta} \text{ and } h = \frac{Nu\ \lambda}{d}\ ,$$

where

- d = coolant channel diameter,
- A = coolant channel cross-sectional area (i.e., flow area),
- η = dynamic viscosity,
- λ = gas thermal conductivity,
- $\dot{m}$ = mass flow rate in the coolant channel,
- Nu = Nusselt number,
- Pr = Prandtl number,
- Re = Reynolds number.

The thermodynamic properties η and λ (determined from correlations in Ref. A.12) are computed at the film temperature taken as the average of the coolant channel surface temperature and the gas temperature.

The core flow is calculated from the circulator speed assuming the volumetric flow to be proportional to circulator speed. Coolant density at the circulator outlet is computed from pressure and circulator outlet temperature according to the gas law (provided in Ref. A.12):

$$\rho = \frac{48.14\ P/T}{\left(1 + 0.4446\ P/T^{1.2}\right)}\ , \qquad (A.21)$$

where ρ is in kilograms per cubic meter, P is in bar, and T is in degrees Kelvin.

References

A.1. J. C. Cleveland, Martin Marietta Energy Systems, Inc. Oak Ridge Natl. Lab., "Analysis of AVR Dynamic Experiments," ORNL/GCR-85/16, September 1985.*

A.2. S. J. Ball, J. C. Cleveland, J. C. Conklin, and R. M. Harrington, "High-Temperature Gas-Cooled Reactor Safety Studies for the Division of Reactor Safety Research, Quarterly Progress Report, Jan. 1–March 13, 1980" NUREG/CR-1521 (ORNL/NUREG/TM-397), August 1980.*

A.3. R. Brogli and R. Froelich, "Space and Spectrum Effects for Rod Removal Transients in an HTGR," *Trans. American Nuclear Society 13* (June–July 1970).†

A.4. E. E. Lewis, *Nuclear Power Reactor Safety*, John Wiley & Sons, New York, 1977.

A.5. Letter from A. J. Neylan, General Atomics, to T. King, Nuclear Regulatory Commission, Subject: Request for MHTGR Information, April 16, 1987.

A.6. J. R. Lamarsh, *Nuclear Reactor Theory*, Addison Wesley Publishing Co., Inc., Reading, Mass., 1966.

A.7. "Decay Heat Power in Light Water Reactors," ANSI/ANS-5.1-1979, American Nuclear Society.†

A.8. Preliminary Safety Information Document for the Standard MHTGR, HTGR-86-024.

A.9. J. C. Cleveland, Union Carbide Corp. Nuclear Div., Oak Ridge Natl. Lab., "CORTAP: A Coupled Neutron Kinetics-Heat Transfer Digital Computer Program for the Dynamic Simulation of the High-Temperature Gas-Cooled Reactor Core," USNRC Report ORNL/NUREG/TM-39, January 1977.*

A.10. J. C. Conklin, Martin Marietta Energy Systems, Inc., Oak Ridge Natl. Lab., "Scaling Analysis of the Coupled Heat Transfer Process in the High-Temperature Gas-Cooled Reactor Core," ORNL/TM-10099, August 1986.*

A.11. S. J. Ball, Union Carbide Corp. Nuclear Div., Oak Ridge Natl. Lab., "ORECA-1: A Digital Computer Code for Simulating the Dynamics of HTGR Cores for Emergency Cooling Analyses, ORNL/TM-5159, April 1976.*

A.12. Kerntechnischer Ausschuss (KTA), Sicherheitstechnische Regel des KTA, gasgekühlten Hochtemperaturreaktoren Teil 1: Berechnung der Helium-Stoffwerke, KTA 3102.1 Fassung 6/78.

*Available for purchase from the National Technical Information Service, Springfield, VA 22161.
†Available in public technical libraries.

Appendix B

Approximate Analytical Methods for Predicting Power and Fuel Temperature Response for Large-Step Reactivity Insertions

For a power excursion resulting from a large-step insertion of reactivity, the following discussion

1. addresses the modeling issue of whether much larger fuel temperature increases would be predicted if a detailed thermal representation of the fuel particles themselves, rather than the simpler homogenized fuel rod compact representation described in Appendix A, were employed in the coupled heat transfer-neutron kinetics analysis; and
2. presents an approximate analytical method for estimating the maximum power and the fuel temperature increase at the time the power reaches its maximum.

During normal full-power steady-state operation, the fuel kernels are only slightly (on the order of 3 to 5°C) hotter than the fuel rod. The first issue above generally arises because the time constant of the fuel particles is very short, and it is anticipated that the predicted fuel temperature response obtained with a model explicitly treating the particles would be larger than that obtained with a model treating a fuel rod compact (assuming the same fuel temperature coefficients) because the model treating the fuel particles themselves would deposit the power into a much smaller mass. Certainly, depositing a given amount of power during a short time into fuel particles would result in higher temperatures than if the same power were deposited over the same time uniformly throughout the fuel rod compact. However, the following calculations show analytically that because of the coupling between temperature feedback and power generation, the fuel rod compact model delays the negative effect of the temperature feedback, resulting in a higher predicted power than would be obtained with a model explicitly treating the fuel particles. Further, these calculations show that the temperature increase predicted by a model representing the homogenized fuel compact is representative of the temperature increase that would be predicted by a particle model, provided the fuel temperature coefficient computed on the basis of fuel particle temperature change is about the same as that computed on the basis of fuel rod compact temperature change, which is reported to be the case for gas-cooled reactors (Ref. B.1).*

The following mathematical derivations make the approximation that the temperature coefficient of reactivity is independent of temperature and treat only the short time interval following a step reactivity insertion during which power generation is large compared to the rate of heat removal from the fuel; that is, the fuel (either the fuel rod compact or the fuel particle) is treated adiabatically. From the general heat conduction equation,

$$\frac{\partial}{\partial t}\left(\rho c_p T\right) = P/V + \nabla \cdot (k\nabla T) \ ;$$

the adiabatic assumption is valid only as long as the power density is much greater than the rate of energy dissipation from the fuel mass, that is, only as long as

$$P/V \gg \left|\nabla \cdot (k\nabla T)\right| \ .$$

Because the initial power, P_o, during steady-state conditions before the step insertion of reactivity can be written as

$$P_o/V = \left|\nabla \cdot (k\nabla T)\right|_{t=0} \ ,$$

and because in a power excursion the temperature gradients and their divergence increase in magnitude, the adiabatic assumption also applies only so long as

$$P \gg P_o \ .$$

In other words, the following applies only to fairly large power excursions and only as long as $P/V \gg |\nabla \cdot (k\nabla T)|$. For a specific case, the length of time for which the adiabatic assumption is valid could be determined by applying the scaling analysis techniques of Ref. B.2 to the general heat conduction equation.

The following will derive an approximate analytical expression for the power, P, as a function of reactivity, ρ. From this, an expression for the maximum power P_{max} during the excursion will be derived. It will be shown that the maximum predicted power is directly proportional to the mass, M, of fuel into which the energy is considered to be deposited in the model. Also, an expression for the power level at the time when the reactivity has returned to zero will be derived. Expressions for the fuel temperature rise at the maximum power, $(\Delta T_f)_{P_{max}}$, and the fuel temperature rise at the time the reactivity has returned to zero $(\Delta T_f)_{\rho=0}$ will be derived, and both will be shown to be independent of the mass of the fuel into which the energy is deposited. This will substantiate the previous claim that a fuel rod compact thermal model, when coupled with the neutron kinetics equations, will predict about the

*Also, private communication between J. C. Cleveland, Oak Ridge National Laboratory, and A. Baxter, General Atomics.

same fuel temperature increase as a fuel particle thermal model, provided the temperature coefficient computed on the basis of fuel rod compact temperature change is about the same as that computed on the basis of fuel particle temperature change.

Step reactivity insertion with $\rho_o < \beta$

The following is based largely on discussions in Ref. B.3. The time-dependent reactivity can be represented as,

$$\rho(t) = \rho_o - \alpha\left[T_f(t) - T_{f,ref}\right] = \rho_o - \alpha\Delta T_f \ , \qquad (B.1)$$

where α is assumed constant and positive (i.e., equal to the magnitude of the negative temperature coefficient). During the time that the adiabatic assumption is valid, the rate of increase in fuel temperature is determined by

$$Mc_p \frac{dT_f(t)}{dt} = P(t) \ . \qquad (B.2)$$

The prompt jump approximation for the neutron kinetics equations with one group of delayed neutrons is

$$P(t) = \frac{\Lambda}{[\beta - \rho(t)]}[\lambda C(t)] \ , \qquad (B.3)$$

and

$$\frac{dC(t)}{dt} = -\lambda C(t) + \frac{\beta}{\Lambda} P(t) \ , \qquad (B.4)$$

where C(t) is the time-dependent delayed neutron precursor concentration, Λ is the prompt neutron generation time, β is the delayed neutron fraction, and $\rho(t)$ is the time-dependent reactivity.

The following will derive an equation for power, P, as a function of reactivity, ρ. Solving Eq. (B.3) for C(t) and using this in Eq. (B.4) gives

$$(\beta - \rho)\frac{dP}{dt} = \left(\lambda\rho + \frac{d\rho}{dt}\right) P \ , \qquad (B.5)$$

From B.1 and B.2,

$$\frac{d\rho}{dt} = -\alpha\frac{dT_f}{dt} = -\frac{\alpha P}{Mc_p} \ .$$

Dividing B.5 by this and replacing $\frac{d\rho}{dt}$ in B.5 with $\frac{-\alpha}{Mc_p}$ P gives

$$\frac{dP}{d\rho} = \left[\lambda\rho - \frac{\alpha P}{Mc_p}\right] \Big/ \left[\frac{\alpha}{Mc_p}(\rho - \beta)\right] , \qquad (B.6)$$

which can also be written as

$$\frac{\alpha}{Mc_p}(\beta - \rho)dP + \left(\lambda\rho - \frac{\alpha P}{Mc_p}\right) d\rho = 0$$

or

$$d\left[\frac{1}{2}\lambda\rho^2 + \frac{\alpha}{Mc_p}(\beta - \rho)\ P\right] = 0 \ .$$

Integration gives

$$\frac{1}{2}\lambda\rho^2 + \frac{\alpha}{Mc_p}(\beta - \rho)\ P = \text{constant} \ . \qquad (B.7)$$

Writing Eq. (B.7) for (ρ_o, P_o), for (ρ, P), and neglecting P_o compared to P (as implied by the adiabatic assumption and discussed earlier) gives the following equation for the power as a function of the reactivity:

$$P = \frac{Mc_p\lambda}{2\alpha}\ \frac{(\rho_o^2 - \rho^2)}{\beta - \rho} \ . \qquad (B.8)$$

With a negative temperature coefficient of reactivity, ρ will continually decrease with time as the fuel heats up, while the power will reach a maximum and then decrease. The maximum power, P_{max}, and the corresponding reactivity $\rho_{P_{max}}$ can be found from Eq. (B.6) by setting $dP/d\rho = 0$, so

$$P_{max} = \frac{Mc_p}{\alpha}\ \lambda\rho_{P_{max}} \ . \qquad (B.9)$$

Writing Eq. (B.8) for P_{max} and $\rho_{P_{max}}$ and substituting for P_{max} from Eq. (B.9) gives

$$\rho_{P_{max}}^2 - 2\beta\ \rho_{P_{max}} + \rho_o^2 = 0 \ ,$$

so

$$\rho_{P_{max}} = \beta \pm \left(\beta^2 - \rho_o^2\right)^{1/2} \ . \qquad (B.10)$$

Selecting the negative root to ensure $\rho < \beta$ gives

$$\rho_{P_{max}} = \beta - \left(\beta^2 - \rho_o^2\right)^{1/2} \ . \qquad (B.11)$$

Then, substituting Eq. (B.11) into Eq. (B.9) gives the following equation for the maximum power during the excursion:

$$P_{max} = \frac{Mc_p}{\alpha}\ \lambda\left[\beta - \left(\beta^2 - \rho_o^2\right)^{1/2}\right] . \qquad (B.12)$$

Because $\rho_{P_{max}} = \rho_o - \alpha(\Delta T_f)_{P_{max}}$, or, using Eq. (B.11),

$$(\Delta T_f)_{P_{max}} = \frac{-1}{\alpha}\left[\beta - \left(\beta^2 - \rho_o^2\right)^{1/2}\right] + \rho_o/\alpha \ . \qquad (B.13)$$

Because $0 < \rho_o < \beta$, the reactivity $\rho_{P_{max}}$, at the time of maximum power, from Eq.(B.11), is still greater than zero. As ρ continues to decrease with continued fuel heatup, it becomes zero and then goes negative. From Eq. (B.8),

$$P(\rho = 0) = \frac{Mc_p\lambda}{2\alpha}\ \frac{\rho_o^2}{\beta}\ . \qquad (B.14)$$

Also,

$$(\Delta T_f)_{\rho=0} = \rho_o/\alpha\ . \qquad (B.15)$$

From Eq. (B.12), note that as expected, P_{max} is larger for smaller temperature coefficients and is independent of Λ. Also, P_{max} is proportional to M, the mass of fuel considered in the model into which the energy is being deposited. This is also true for the power when ρ returns to zero, $P(\rho = 0)$, from Eq. (B.14). Therefore, a homogenized fuel rod compact model, with the energy assumed to be deposited throughout the entire fuel compact, will give a conservative prediction for P_{max} and for $P(\rho = 0)$ (for the same α). The most interesting observation is that $(\Delta T_f)_{P_{max}}$ in Eq. (B.13) and $(\Delta T_f)_{\rho=0}$ in Eq. (B.15) are dependent on α and ρ_o, as expected, but are not dependent on the mass of fuel into which the energy is assumed to be deposited. Therefore, a model treating explicitly the fuel particles and depositing all the energy into the particles would yield the same $(\Delta T_f)_{P_{max}}$ and $(\Delta T_f)_{\rho=0}$ as a model that treats the homogenized fuel rod compact, providing the fuel temperature coefficients of reactivity computed on the different bases are essentially the same. Further, as T_f increases beyond $T_{f,ref} + (\Delta T_f)_{\rho=0}$, one would not expect a particle model to yield higher temperatures than a homogenized fuel rod compact model, especially because the fuel compact model is conservative from the standpoint of predicted power.

Step reactivity insertion with $\rho_o > \beta$

The following is based largely on discussions in Refs. B.3–B.5. Power excursions resulting from step reactivity insertions greater than $1.00 are characterized by a short burst followed by a slowly decaying tail. The burst characteristics are determined by the prompt neutron behavior. Because of the large number of precursors formed during the burst, the long tail results from the neutrons produced by decay of these precursors. The power burst is so rapid that the delayed neutron precursor half-lives are long compared to the burst time, so, effectively, the decay constants λ_i for precursors are zero for this short time. During the burst portion of the transient, the power generation is very large compared to the rate of heat removal from the fuel; therefore, an adiabatic model is appropriate for a short time interval.

The relevant equations are

$$\frac{dP}{dt} = \frac{\rho - \beta}{\Lambda}\ P\ , \qquad (B.16)$$

$$\frac{dT_f}{dt} = \frac{1}{Mc_p}\ P\ , \qquad (B.17)$$

(note that this adiabatic assumption can hold only as long as $P \gg P_o$) and

$$\rho(t) = \rho_o - \alpha\left[T_f(t) - T_{f,ref}\right]\ , \qquad (B.18)$$

where the temperature coefficient of reactivity is again assumed to be independent of temperature (and α is positive representing the magnitude of the negative temperature coefficient). The following will derive an equation for the power, P, as a function of reactivity, ρ.

From Eqs. (B.18) and (B.17)

$$\frac{d\rho}{dt} = -\alpha\frac{dT_f}{dt} = \frac{-\alpha}{Mc_p}\ P\ .$$

Dividing this into Eq. (B.16) gives

$$\frac{dP}{d\rho} = \frac{Mc_p}{\alpha} = \frac{(\beta - \rho)}{\Lambda}\ . \qquad (B.19)$$

Integrating and assuming that the initial power is small compared to the power during the burst phase of the excursion gives the power as a function of reactivity:

$$P = \frac{Mc_p}{\alpha\Lambda}\left[\beta(\rho - \rho_o) - \frac{1}{2}\left(\rho^2 - \rho_o^2\right)\right]\ . \qquad (B.20)$$

Note from Eqs. (B.17) and (B.18) that ρ is at its maximum ($\rho = \rho_o$) at $t = 0$ and continually decreases thereafter because of the adiabatic fuel heatup. Thus, $d\rho$ is always negative in Eq. (B.19). Initially $\rho = \rho_o > \beta$, and until ρ becomes less than β, the right-hand side of Eq. (B.19) is negative. Therefore, until ρ becomes less than β, dP is positive. After ρ becomes less than β, the right-hand side of Eq. (B.19) is positive, making dP negative because $d\rho$ is always negative. All this means that P reaches its maximum when $\rho = \beta$ (i.e., the reactor is no longer supercritical on prompt neutrons). [Note that from Eq. (B.20), $d^2P/d\rho^2$ is always negative, which means that P has a maximum where $dP/d\rho = 0$. That P has a maximum at $\rho = \beta$ (given that delayed neutrons can be neglected) can also be seen from Eq. (B.16).]

So, from Eq. (B.20), with $\rho = \beta$,

$$P_{max} = \frac{Mc_p}{2\alpha\Lambda}\left[(\beta - \rho_o)^2\right]\ . \qquad (B.21)$$

Note that as expected, P_{max} is larger for smaller α, smaller Λ, and larger M. (Note that in the previous section with the assumption that $\rho_o < \beta$, P_{max} was independent of Λ.) The larger the mass into which the power is deposited delays the negative response of the fuel temperature feedback,

resulting in larger maximum power. When ρ decreases further and returns to zero, the power [from Eq. (B.20)] is

$$P(\rho = 0) = \frac{Mc_p}{2\alpha\Lambda}\left[\rho_o^2 - 2\beta\rho_o\right], \qquad (B.22)$$

which is less than P_{max} by an amount equal to $\frac{Mc_p}{2\alpha\Lambda}\beta^2$.

Also, note that when the power is at its maximum,

$$\rho_{P_{max}} = \beta = \rho_o - \alpha(\Delta T_f)_{P_{max}},$$

where $(\Delta T_f)_{P_{max}}$ is the temperature increase at the time the power reaches its maximum value. So

$$(\Delta T_f)_{P_{max}} = \frac{(\rho_o - \beta)}{\alpha}, \qquad (B.23)$$

which is independent of the mass of the fuel into which the power is deposited. The temperature increase necessary to return ρ to zero, $(\Delta T_f)_{f=0}$, is

$$(\Delta T_f)_{\rho=0} = \rho_o/\alpha, \qquad (B.24)$$

which is also independent of the mass of the fuel into which the power is deposited. Therefore, again from Eqs. (B.21) and (B.22), a model representing the homogenized fuel rod compact will give a conservative prediction for the power relative to a model that assumes all the power is deposited directly into the fuel particles. Furthermore, the predicted temperature increases from Eqs. (B.23) and (B.24) are independent of the mass and therefore are representative of temperature increases that would be predicted by a particle model, provided the fuel temperature coefficient computed on the basis of particle temperature change is about the same as that computed on the basis of fuel rod compact temperature change.

References

B.1. K. Tokuhara et al., "Determination of Temperature Coefficients and Kinetics Parameters for the HTTR Safety Analysis," *Proceedings of IAEA Specialists' Meeting on Uncertainties in Physics Calculations for Gas-Cooled Reactor Cores, Villigen, Switzerland*, IWGGCR/24, IAEA Vienna, May 1991.

B.2. J. C. Conklin, Martin Marietta Energy Systems, Inc., Oak Ridge Natl. Lab., "Scaling Analysis of the Coupled Heat Transfer Process in the High Temperature Gas-Cooled Reactor Core," ORNL/TM-10099, August 1986.*

B.3. H. F. Lutz, Lawrence Livermore National Laboratory, "Nuclear Criticality Safety Assessment Calculations: Part 1. Calculating Power Histories in Nuclear Excursions," M-164, June 1985.*

B.4. E. E. Lewis, "*Nuclear Power Reactor Safety*," John Wiley and Sons, New York, 1977.

B.5. T. J. Thompson and J. C. Beckerley, *The Technology of Nuclear Reactor Safety, Volume 1, Reactor Physics and Control*, The MIT Press, Massachusetts Institute of Technology, Cambridge, Mass., 1973.

*Available for purchase from the National Technical Information Service, Springfield, VA 22161.

NUREG/CR-5922
ORNL/TM-12179
Dist. Category R7, R8

INTERNAL DISTRIBUTION

1. S. J. Ball
2. W. P. Barthold
3–7. J. C. Cleveland
8. J. C. Conklin
9. E. C. Fox
10. S. R. Greene
11. F. J. Homan
12. J. E. Jones Jr.
13. H. Jones
14. H. T. Kerr
15. T. S. Kress
16. D. L. Moses
17–18. C. E. Pugh
19. O. L. Smith
20. C. C. Southmayd
21. O. M. Stansfield
22. J. D. White
23. R. P. Wichner
24. B. A. Worley
25. A. Zucker
26. ORNL Patent Section
27. Central Research Library
28. Document Reference Section
29–30. Laboratory Records Department
31. Laboratory Records (RC)

EXTERNAL DISTRIBUTION

32. B. W. Sheron, Director, Division of Regulatory Applications, Office of Nuclear Regulatory Research, U.S. Nuclear Regulatory Commission, Washington, DC 20555
33. M. A. Bender, Nuclear Regulatory Commission, Computer Review, Washington, DC 20555
34. D. E. Carlson, Office of Nuclear Regulatory Research, U.S. Nuclear Regulatory Commission, NL/S 169, Washington, DC 20555
35. F. C. Chen, U.S. Department of Energy, NP-62, Washington, DC 20585
36. J. N. Donohew, Office of Nuclear Reactor Regulation, U.S. Nuclear Regulatory Commission, Washington, DC 20555
37. E. F. Goodwin, Office of Nuclear Reactor Regulation, U.S. Nuclear Regulatory Commission, Washington, DC 20555
38. J. M. Kendall, PDCO, MHTGR-NE, P.O. 85608, San Diego, CA 92138
39. Peter G. Kroeger, Brookhaven National Laboratory, Upton, NY 11973
40. C. Rogriguez, CEGA, MS-236, P. O. Box 85608, San Diego, CA 92138-5608
41. Zoltan Rosztoczy, Office of Nuclear Regulatory Research, U.S. Nuclear Regulatory Commission, Washington, DC 20555
42. Peter M. Williams, Director, Division of HTGRs, NE-451, U.S. Department of Energy, Washington, DC 20585
43. Office of Assistant Manager for Energy Research and Development, Department of Energy, Oak Ridge Operations, Oak Ridge, TN 37831

44–45. Office of Scientific and Technical Information, P.O. Box 62, Oak Ridge, TN 37831

NRC FORM 335 (2-89) NRCM 1102, 3201, 3202

U.S. NUCLEAR REGULATORY COMMISSION

BIBLIOGRAPHIC DATA SHEET

(See instructions on the reverse)

1. REPORT NUMBER (Assigned by NRC, Add Vol., Supp., Rev., and Addendum Numbers, if any.)

NUREG/CR-5922
ORNL/TM-12179

2. TITLE AND SUBTITLE

Modular High-Temperature Gas-Cooled Reactor Short-Term Thermal Response to Flow and Reactivity Transients

3. DATE REPORT PUBLISHED

MONTH	YEAR
February	1993

4. FIN OR GRANT NUMBER

A9477

5. AUTHOR(S)

J. C. Cleveland

6. TYPE OF REPORT

Technical

7. PERIOD COVERED (Inclusive Dates)

8. PERFORMING ORGANIZATION – NAME AND ADDRESS (If NRC, provide Division, Office or Region, U.S. Nuclear Regulatory Commission, and mailing address; if contractor, provide name and mailing address.)

Oak Ridge National Laboratory
Oak Ridge, TN 37831

9. SPONSORING ORGANIZATION – NAME AND ADDRESS (If NRC, type "Same as above"; if contractor, provide NRC Division, Office or Region, U.S. Nuclear Regulatory Commission, and mailing address.)

Division of Systems Research
Office of Nuclear Regulatory Research
U.S. Nuclear Regulatory Commission
Washington, DC 20555

10. SUPPLEMENTARY NOTES

11. ABSTRACT (200 words or less)

The research reported here has been conducted at the Oak Ridge National Laboratory for the Nuclear Regulatory Commission's Division of Regulatory Applications of the Office of Nuclear Regulatory Research. The short-term thermal response of the Modular High-Temperature Gas-Cooled Reactor (MHTGR) is analyzed for a range of flow and reactivity transients. These transients include loss of forced circulation without scram, spurious withdrawal of a control rod group, moisture ingress, control rod and control rod group ejections, and a rapid core cooling event. For each event analyzed, an event description, a discussion of the analysis approach and assumptions, and results are presented. When possible, results of these analyses are compared with those presented by the designers in the MHTGR Probabilistic Risk Assessment. The importance of inherent safety features is illustrated, and conclusions are presented regarding the safety performance of the MHTGR. Recommendations are made for a more in-depth examination of MHTGR response for some of the analyzed transients. The coupled heat transfer-neutron kinetics model is described in detail in Appendix A.

12. KEY WORDS/DESCRIPTORS (List words or phrases that will assist researchers in locating the report.)

MHTGR	Reactivity
Gas-cooled reactors	Safety
Flow	Neutron kinetics

13. AVAILABILITY STATEMENT

Unlimited

14. SECURITY CLASSIFICATION

(This Page)

Unclassified

(This Report)

Unclassified

15. NUMBER OF PAGES

16. PRICE

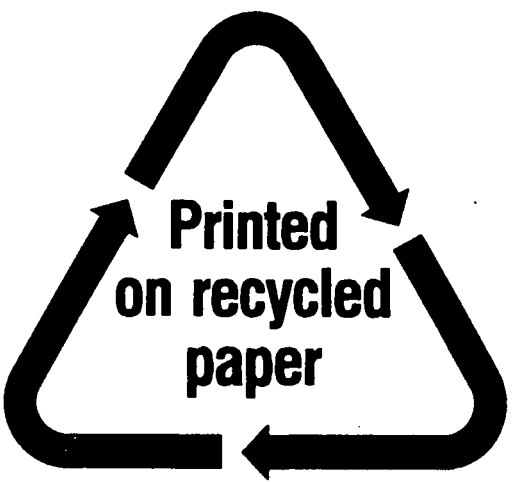

Federal Recycling Program